AGU PUBLICATIONS

Water Resources Research

RESEARCH ARTICLE

10.1002/2017WR021094

Probable Maximum Precipitation in the U.S. Pacific Northwest in a Changing Climate

APPROVED

Xiaodong Chen[1], Faisal Hossain[1], and L. Ruby Leung[2] AQ5

[1]Department of Civil and Environmental Engineering, University of Washington, Seattle, WA, USA, [2]Atmospheric Sciences and Global Change Division, Pacific Northwest National Laboratory, Richland, WA, USA

Key Points:
- Combining traditional PMP estimation approach with modern climate science can provide PMP estimates consistent with current practice
- In the worst climate scenario (RCP8.5), PMP in the PNW region is projected to increase by about 50% ± 30% by 2099 relative to the 2016 level
- PMP presents larger uncertainty than extreme precipitation

Supporting Information:
- Supporting Information S1

Correspondence to:
F. Hossain,
fhossain@uw.edu

Citation:
Chen, X., Hossain, F., & Leung, L. R. (2017). Probable Maximum Precipitation in the U.S. Pacific Northwest in a changing climate. *Water Resources Research*, *53*. https://doi.org/10.1002/2017WR021094

Received 10 MAY 2017
Accepted 28 OCT 2017
Accepted article online 3 NOV 2017

Abstract The safety of large and aging water infrastructures is gaining attention in water management given the accelerated rate of change in landscape, climate, and society. In current engineering practice, such safety is ensured by the design of infrastructure for the Probable Maximum Precipitation (PMP). Recently, several numerical modeling approaches have been proposed to modernize the conventional and ad hoc PMP estimation approach. However, the underlying physics have not been fully investigated and thus differing PMP estimates are sometimes obtained without physics-based interpretations. In this study, we present a hybrid approach that takes advantage of both traditional engineering practice and modern climate science to estimate PMP for current and future climate conditions. The traditional PMP approach is modified and applied to five statistically downscaled CMIP5 model outputs, producing an ensemble of PMP estimates in the Pacific Northwest (PNW) during the historical (1970–2016) and future (2050–2099) time periods. The hybrid approach produced consistent historical PMP estimates as the traditional estimates. PMP in the PNW will increase by 50% ± 30% of the current design PMP by 2099 under the RCP8.5 scenario. Most of the increase is caused by warming, which mainly affects moisture availability through increased sea surface temperature, with minor contributions from changes in storm efficiency in the future. Moist track change tends to reduce the future PMP. Compared with extreme precipitation, PMP exhibits higher internal variability. Thus, long-time records of high-quality data in both precipitation and related meteorological fields (temperature, wind fields) are required to reduce uncertainties in the ensemble PMP estimates.

Plain Language Summary In this study, the hybrid approach is used to reconstruct the PMP in the Pacific Northwest region and investigate the likely future change in PMP under projected climate change by climate models. Our research questions are as follows. (1) What are the PMP estimates in the U.S. PNW region based on climate science and current engineering convention? (2) How will such PMP estimates change in the future in the PNW region and what are the contributions of various climate factors to the PMP change?

1. Introduction

In the past century, numerous water infrastructures have been built to facilitate irrigation, hydropower generation, transportation, and municipal water use. In a changing climate, extreme precipitation events are projected to be more frequent and intense, exceeding known historical records (Allan & Soden, 2008; Kunkel et al., 2013a; Trenberth et al., 2003). Along with structural safety, the hydrologic safety of water infrastructures is now therefore gaining more attention, since overtopping or embankment failure would bring catastrophic human and societal loss (Casagli et al., 2006; Evans et al., 2000; Lane, 2013). For example, the structural damage to both the primary and the emergency spillways of the Oroville Dam in California, which could have been exacerbated by hydrologic failure, during a series of heavy rainstorms in February 2017 led to an evacuation of over 188,000 downstream residents (Vahedifard et al., 2017).

Most of the water infrastructures, especially the hazardous ones located upstream of population centers, are often designed considering the standard Probable Maximum Precipitation (PMP; Hossain et al., 2012). PMP, by its definition, is the theoretical maximum precipitation that a given watershed can receive in a given duration of time (World Meteorological Organization [WMO], 1986). WMO suggests several methods for PMP estimation: statistical method, generalized method, transposition method, and moisture maximization method (Hershfield, 1965; Rakhecha & Kennedy, 1985; Rakhecha & Singh, 2009; WMO, 1986). The moisture maximization approach is the recommended method in the U.S. NOAA has published a series of Hydro-Meteorological Reports (HMRs) that provide instructions for PMP estimation in various climatological regions across the U.S. (Schreiner & Riedel, 1978). The moisture maximization method estimates PMP as $PMP = p \times PWM/PW$, where p is the observed precipitation, PW is the observed precipitable water, and PWM is the climatologically maximum precipitable water (estimated from surface dew point temperature assuming hydrostatic conditions).

The moisture maximization method has been criticized in several studies as being insufficiently grounded in physics (Abbs, 1999). Also, the accuracy of this approach heavily relies on availability and quality of observation data, which makes PMP estimation less reliable in regions where sufficient observation has not been obtained. Traditionally, PMP is treated as a static value, estimated using long-term precipitation and related meteorological data (such as humidity, temperature, and winds). The static nature of PMP estimation has been questioned as global warming can lead to changing precipitation patterns. Nonstationary analyses of extreme precipitation also suggest that PMP, an upper bound of extreme precipitation, is likely to change in the future (Cheng & AghaKouchak, 2014; Cheng et al., 2014; Gao et al., 2016; Wi et al., 2016).

In recent years, two significant advancements have been made to modernize PMP estimation used in engineering practice. One of them is the ability to derive uncertainty associated with PMP estimation (Micovic et al., 2015; Salas et al., 2014). Another advancement is the introduction of numerical atmospheric models to enable a more physics-based estimation of PMP (Chen et al., 2017; Chen & Hossain, 2016; Ishida et al., 2015; Ohara et al., 2011; Tan, 2010). In atmospheric model-based estimates, PMP is obtained by modifying the initial/boundary conditions of extreme precipitation event simulations, such as increased moisture availability (usually by setting relative humidity RH to 100%), increased air temperature, spatially shifted initial/boundary conditions, or artificially generated convergent wind fields. Most studies focused on the construction of PMP from various atmospheric reanalysis data, although climate model data have also been explored (Beauchamp et al., 2013; Lee et al., 2017; Ohara et al., 2011; Rastogi et al., 2017; Rouhani & Leconte, 2016; Rousseau et al., 2014; Tan, 2010). These studies suggest that carefully selected climate data, such as the CMIP5 data, may have value for historical PMP estimation. However, care should be taken in selecting climate models, as climate simulations (such as CMIP5) exhibit a wide range of precipitation estimation (Sheffield et al., 2013). Alternatively, regional climate model output can be used for PMP estimation with the advantage of providing more spatially resolved precipitation features. These studies reveal the potential of climate projections to quantify the sensitivity of PMP to climate change (Beauchamp et al., 2013; Rastogi et al., 2017; Rousseau et al., 2014).

Up to now, such model-based approaches have not been widely validated, and their physical basis has not been thoroughly established. By modifying different variables in the simulations, the modeling approaches implicitly assume that extreme precipitation will be more sensitive to the variables modified. For example, the RH maximization approach assumes that storm magnitude is more sensitive to the RH level, while a wind perturbation approach assumes that storm is more sensitive to the moisture convergence. Several other approaches, such as the spatial shift of initial/boundary conditions (Ishida et al., 2015; Ohara et al., 2011), produce results that are even harder to interpret. From the modelling perspective, moving the atmospheric boundary condition spatially induces a shift in the land surface condition. In regions where surface heterogeneity is an important driver of precipitation variability, shifting the atmospheric boundary condition can result in drastic changes in the storm characteristics and hence PMP estimation.

The aforementioned approaches have not been comprehensively compared to the traditional estimates up to now, and the PMP estimation results often differ from traditional values that have been used in the infrastructure design stage. Such inconsistency makes it hard to use the new results to reevaluate the safety of infrastructures. Lastly, most of the modelling studies focused on selected watersheds, making it harder to derive general guidelines for engineering designing across regions (an exception is the study by Rastogi et al. (2017), which focused on building the depth-area-duration curves).

The traditional engineering approach takes all the information from historical observations, while an atmospheric model-based physical approach accounts for all dynamical and physical processes that influence the storms. Due to a significant gap between these two contrasting approaches, it is hard for the respective communities (i.e., ~~engineering~~ for conventional PMP and scientists for model-based PMP) to communicate the needs and constraints for collaborative advancements. This is especially important when evaluating the sensitivity of PMP to climate change since the reference (i.e., historical PMP) has been estimated quite differently. Therefore, it is important to bridge the gap between the two contrasting types of estimation. In this study, a hybrid approach of applying the traditional methodology to climate model outputs is proposed. Climate model outputs provide long-term archives of extreme events, which would improve estimates of extreme events and help reveal the climatic trend of PMP estimate. The nonstationary issues can therefore be addressed by estimating PMP using future climate projections. Most importantly, the availability of ensemble climate model output (e.g., ~30 models used in IPCC AR5) allows derivation of ensemble PMP estimates useful for evaluating the statistical significance of future changes in PMP. An added benefit of the hybrid approach is the ease of use by those who are already familiar with the conventional approach used in the current engineering practice. No complex and computationally intensive modeling resources are required in our proposed approach as model outputs are readily available from the climate modeling community.

In this study, the hybrid approach is used to reconstruct the PMP in the Pacific Northwest region and investigate the likely future change in PMP under projected climate change by climate models. As overviewed by Hossain et al. (2012), most of the large, high-hazards dams across the U.S. are designed under PMP or PMF (probable maximum flood, the flood event under PMP scenario). Therefore, to check the future safety of such high-hazards dams and reservoirs, ~~3-day~~ PMP is prioritized in this study. Our research questions are as follows. (1) What are the PMP estimates in the U.S. PNW region based on climate science and current engineering convention? (2) How will such PMP estimates change in the future in the PNW region and what are the contributions of various climate factors to the PMP change?

2. Data and Methods

In this study, we focus on the Pacific Northwest, as shown in Figure 1. Figure 1a shows the topography from ETOPO1 database (Amante & Eakins, 2009) in the study domain, which features the Cascade Range along the coast. Extreme precipitation in this region is mainly triggered by atmospheric river events that transport significant atmospheric moisture from the Pacific Ocean (Dettinger, 2011; Leung & Qian, 2009; Neiman et al., 2011; Ralph et al., 2011). As storms approach from the Pacific Ocean, extreme precipitation in this region shows a distinctive signature across the Cascade Range as abundant moisture condenses and is converted to precipitation when air mass is lifted over the mountain, so precipitation is much stronger on the west or windward side of the Range. Figure 1 shows the PMP estimation from this study for each Hydrological Unit (HU) in Pacific Northwest. HU is developed by US Geological Survey (USGS) to define various hydrological characteristics such as lakes, watersheds or catchments (Seaber et al., 1987). In this study the eight-

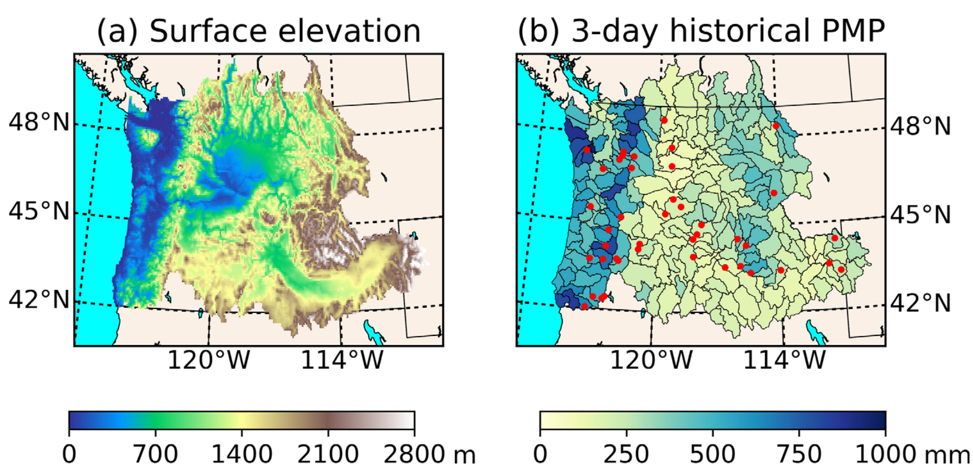

Figure 1. Pacific Northwest (PNW) domain in this study. (a) The surface elevation in the PNW study domain. (b) Highlights all the Hydrological Unit (HU8) basins in the PNW. The colors show the hybrid PMP estimation from this study. The red dots denote locations where PMP estimation is available in Hydrometeorological Report No. 57 (HMR57). These HMR57 PMP values are shown in Figure 5.

AGU Water Resources Research 10.1002/2017WR021094

digit HU is used, and is referred to as HU8 below. The red dots denote the locations of dams/reservoirs where PMP estimations are available in HMR57 (HMR for Pacific Northwest region). These values were later used to evaluate the PMP estimations from this study.

Our hybrid PMP estimation uses five CMIP5 model results for PMP estimation, and in total ~~10~~ CMIP5 models are used for robust uncertainty estimation (Mote et al., 2011). The PMP estimation approach follows the HMR57 instructions. Necessary modifications are made to adapt climate model data and the trajectory procedure that is modernized using the HYSPLIT (Hybrid Single-Particle Lagrangian Integrated Trajectory) model. Details about the data and the method are presented below. We chose 1970–2016 as the historical PMP study period and 2050–2099 RCP8.5 scenario as the future PMP study period.

2.1. CMIP5 Climate Model Data

Five CMIP5 models are used for ensemble estimation of PMP, and an additional five models are also used to estimate the uncertainty range of PMP estimation. Their information is summarized in Table 1. These ten models were selected from the comprehensive evaluation of CMIP5 models over the PNW region using multiple metrics (Rupp et al., 2013), and they cover a wide range of model performance from best to average. The five models used in PMP estimation were selected based on their performance in capturing the statistics of atmospheric river frequency (Gao et al., 2015). This selection is discussed in detail in section 3. These five models also cover a range of model resolution (between 0.75° and 2°), so the impact of climate model resolution on the PMP estimation can also be evaluated.

For the two study periods, 6-hourly/daily data are used. They include 3-D data of horizontal and vertical wind, temperature, geopotential height, relative humidity, and 2-D data of 10 m wind, 2 m temperature, and sea surface temperature. Statistically downscaled data produced by the Localized Constructed Analogs (LOCA) method are used to provide high-resolution daily precipitation. Compared with dynamical downscaling, the statistically downscaling techniques have two unique characteristics. (1) They save significant amount of computational time compared with dynamically downscaled data, and they are free from uncertainty that are caused by various parameterization schemes in the numerical models. (2) They smoothen the bias embedded in the current coarse-resolution GCMs and make more GCM usable for robust ensemble estimation.

This 1/16° data set covers 32 CMIP5 models across the contiguous U.S. during 1950–2099. This data set is developed at the Scripps Institution of Oceanography and is used in the Fourth National Climate Assessment and other climate change impact studies (Pierce et al., 2014, 2015; Tarroja et al., 2016). Our evaluation indicates that for the historical precipitation (1981–2016), the LOCA-downscaled precipitation reproduces the observed spatial-temporal variations of precipitation well and is close to gauge-based data sets such as

Table 1
Information on the 10 Selected CMIP5 Models Used in This Study

Model	Modeling center	Horizontal grid size (atmospheric)	Number of vertical layers
ACCESS1.0	Commonwealth Scientific and Industrial Research Organization (CSIRO) and Bureau of Meteorology (BOM), Australia	1.25 × 1.875 (N96)	38
CMCC-CM	Centro Euro-Mediterraneo per I Cambiamenti Climatici	0.75 × 0.75 (T159)	31
CNRM-CM5	Centre National de Recherches Météorologiques/Centre Européen de Recherche et Formation Avancée en Calcul Scientifique	1.4 × 1.4 (TL127)	31
GFDL-ESM2G	NOAA Geophysical Fluid Dynamics Laboratory	2 × 2.5 (M45L24)	24
MPI-ESM-LR	Max-Planck-Institut für Meteorologie (Max Planck Institute for Meteorology)	1.865 × 1.875 (T63)	47
ACCESS1–3	Commonwealth Scientific and Industrial Research Organization (CSIRO) and Bureau of Meteorology (BOM), Australia	1.25 × 1.875 (N96)	38
CanESM2	Canadian Center for Climate Modelling and Analysis	2.7906 × 2.8125 (T63)	35
HadGEM2-CC	UK Met Office Hadley Centre	1.875 × 1.25 (N96)	60
HadGEM2-ES	UK Met Office Hadley Centre	1.875 × 1.25 (N96)	38
MIROC5	University of Tokyo, National Institute for Environmental Studies, and Japan Agency for Marine-Earth Science and Technology	1.4 × 1.4 (T85)	40

Note: For all of the 10 models, the r1i1p1 ensemble member is used for historical (1970–2005) and RCP8.5 (2006–2016 and 2050–2099) periods. The first 5 models are used for PMP estimation; all 10 models are used to estimate the uncertainty in the PMP.

Water Resources Research 10.1002/2017WR021094

the PRISM gridded climatology data set (see section 4.3 for detailed evaluation; Daly et al., 1994). The LOCA method includes a bias correction step and a spatial downscaling step using historical analog (Pierce et al., 2014). The LOCA downscaling with observed precipitation (in this case the Livneh data) handles the orographic effect on precipitation satisfactorily, as reflected in the historical analog. Therefore, the storm separation method (SSM) as suggested in HMR57 is no longer needed. The RCP8.5 scenario is chosen for this study, as it is closest to the emission in the recent years (Peters et al., 2013). Climate warming will directly affect precipitable water (*PW*) level as the atmospheric moisture holding capacity increases with temperature following the Clausius-Clapeyron relationship (e.g., Berg et al., 2013; Ivancic & Shaw, 2016; Lenderink & van Meijgaard, 2008; Pall et al., 2007). Also, the "storm efficiency" (*p/PW*, i.e., how much air moisture will be converted to actual precipitation) may change through changes in vertical velocity. As the business-as-usual scenario, RCP8.5 features the largest warming through 2100, so it provides an upper bound useful for investigating the maximum possible change in extreme precipitation (thus PMP) for infrastructure risk concern in the future.

2.2. HYSPLIT Back Trajectory Analysis

The HYSPLIT model was developed by NOAA's Air Resources Laboratory as a system for simulating air parcel transport, dispersion, and deposition process (Draxler & Hess, 1997, 1998; Stein et al., 2015). It has been widely used in the studies of air pollutants, wind-blown dust as well as air moisture transport (Ashrafi et al., 2014; Chen et al., 2013; Cohen et al., 2004; Draxler & Rolph, 2012; Stein et al., 2007). HYSPLIT has demonstrated its performance in evaluations against observations from several field campaigns (Graziani et al., 1998; Ngan et al., 2015). In hydrometeorology, HYSPLIT is often used to identify the origin and pathway of moisture transport in studies of different meteorological events (Brimelow & Reuter, 2005; Li et al., 2016). HYSPLIT uses 3-D meteorological fields to calculate tracks of air parcels either in a forward mode or backward mode, and it is used here with the CMIP5 model output (6-hourly or daily, at the finest temporal resolution available) for back trajectory calculation.

2.3. PMP Estimation Method

In this study, we combine the traditional PMP estimation method with climate model data, so our historical PMP estimations are consistent with the established numbers in practice as well as usable for projection into the future. AQ2

$$PMP = p \cdot \frac{PWM}{PW} \tag{1}$$

PMP is usually estimated using equation (1), which maximizes the observed total precipitation p using the climatologically maximum precipitable water *PWM*. In most regions, precipitable water is estimated from local surface dew point temperature, following the relationship in WMO (1986). Given that extreme precipitations in the PNW are often induced by atmospheric rivers that originate from the warm tropical/subtropical oceans, precipitable water in PNW storms is estimated using sea surface temperature (SST) in practice (i.e., the surface dew point temperature is replaced by SST in the precipitable water calculation). From our experiments, most of the air mass contributing to extreme storms originates from within the box between 15°N and 55°N, and from 180°W to the U.S. west coast. Below is a description of the steps to make ~~3 day~~ PMP estimation using the hybrid approach, as illustrated in Figure 2. F2

Step 1. Determine the extreme storm events in the study watershed (Figure 2a). In this study, the LOCA-downscaled precipitation data provide the daily total precipitation over the watershed, and the top 2% most severe ~~3 day~~ precipitation events (~100 storm events in each watershed for a ~~50 year~~ period) can be determined based on the total precipitation amount (Figure 2b).

Step 2. From the precipitation data, determine the storm center as the location of maximum precipitation. This is done by checking the three daily precipitation maps from the LOCA-downscaled data set (Figure 2c).

Step 3. From the storm center location/time, use the wind charts to track the air mass of the storm backward till the beginning of the ~~3 day~~ period. If the end point of the back trajectory is over the ocean, SST at that point is taken to reflect the moisture availability (in the same way that local surface dew point temperature is used in the other climatological regions). In this study, this step was modified to adapt to the HYSPLIT model as elaborated below.

AGU Water Resources Research 10.1002/2017WR021094

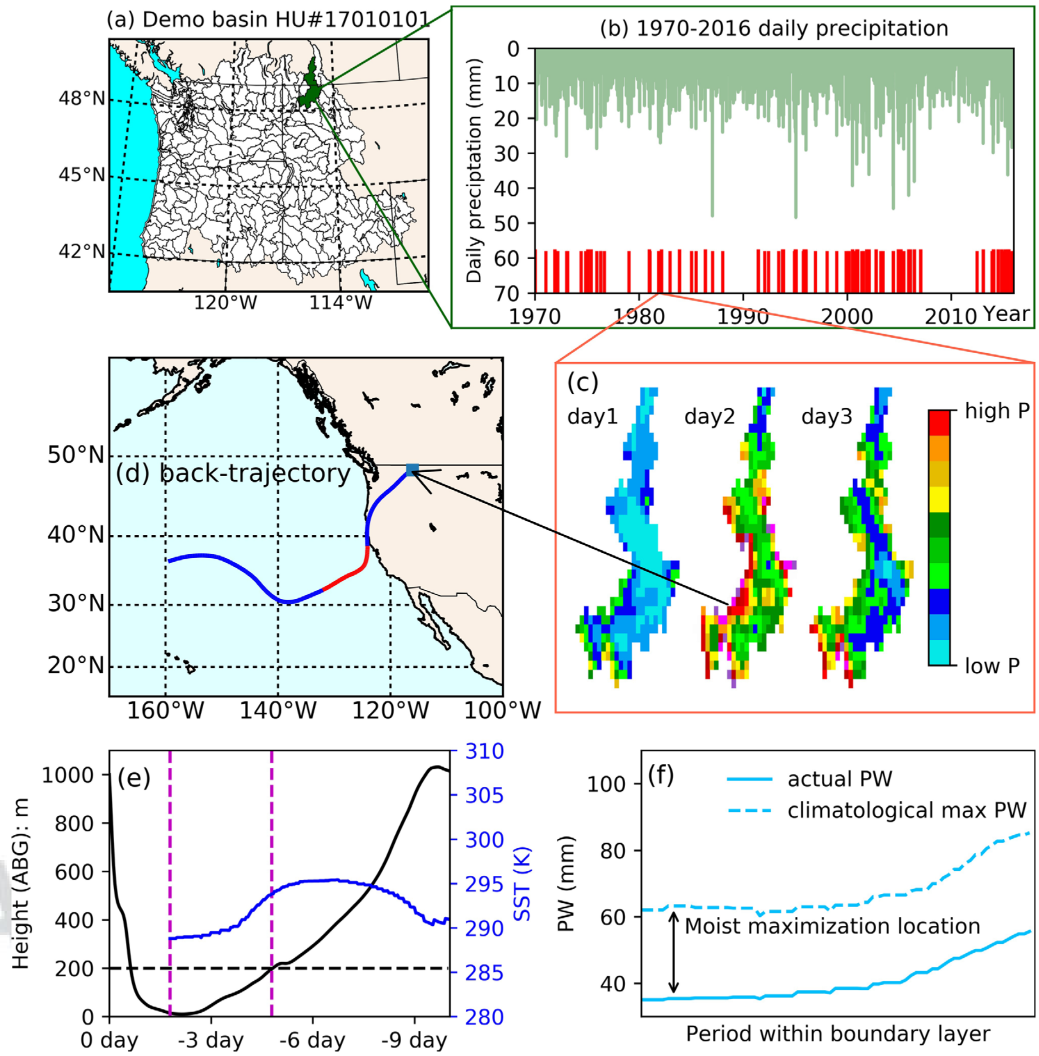

Figure 2. Schematic of the hybrid PMP estimation approach. (a) The location of the demo watershed (Hydrological Unit 17010101), (b) the historical daily precipitation from LOCA-downscaled CNRM-CM5 data between 1970 and 2006, and the top 100 events for PMP estimation is determined using ~~3-day~~ total precipitation. For each event, we pick out (c) the grid/day with the most daily precipitation as the storm center, and (d) release an air parcel at 1,000 m height from this location/date in HYSPLIT. (e) The air parcel is tracked for 10 days, and the height/SST along the track is recorded. When the air parcel is within 200 m height boundary layer above the ocean (the purple dashed line window in Figure 2e), moisture maximization is applied, and (f) the maximum maximization ratio is used to maximize this storm to one MP estimation. PMP is then estimated as the greatest MP based on these 100 events. More details are provided in section 2.3.

An air mass is released at 1,000 m above the ground at the location/date determined in step 2. The air mass at 1,000 m above the surface is representative of the air that provides the moisture content for condensation and precipitation. This air mass is then tracked backward, and allowed to move both horizontally and vertically (Figure 2d). Once the air mass is over the ocean, its path is recorded as long as the air mass is within the ocean boundary layer (200 m in this study, Figure 2e). SST data are taken from this path. Note that our CMIP5 SST data have been smoothed to a $2^\circ \times 2^\circ$ box (instead of using the GCM grid point SST value) to be more representative of the spatial scale of air-sea interaction. In the HYSPLIT model, the air parcels are tracked for 10 days, corresponding to the average residence time of water vapor in the air (Chen et al., 2012; Huang & Cui, 2015; Numaguti, 1999). In our case, since at each watershed we checked $\sim$100 extreme precipitation events, a small fraction ($<$3%) of the back trajectories may end up on the land, and these events are taken out from the estimation. Our check indicates that all the big storms (i.e., top 20) produced end points over the ocean, so no major extreme storms are missing in the estimation.

Water Resources Research 10.1002/2017WR021094

Step 4. At the end point of the back trajectory, climatologically maximum SST (i.e., the maximum SST in the duration of 1970–2016, or 2050–2099) is taken and used to maximize the moisture availability of the rainstorm. In HYSPLT model, since we do not track how much moisture comes from the ocean at each time step, we calculate the ratio between the maximum moisture availability and the actual atmospheric moisture along the trajectory, and take the maximum ratio to maximize the LOCA ~~3 day~~ precipitation for maximum precipitation (MP) estimation (Figure 2f).

Following steps 2–4, one MP is obtained for each extreme event following equation (2), where observed precipitation p is maximized using PW estimated from the event SST and PWM estimated from climatologically maximum SST. The MP calculation is done at the location where precipitation would be maximized most (i.e., highest PMW/PW ratio along the moist track). The relationship between SST and PW is provided in WMO (1986). Next, the largest MP among the top 2% storm events determined in step 1 is taken as the ~~3 day~~ PMP estimation for the watershed. Using the LOCA-downscaled precipitation with the corresponding CMIP5 wind and SST fields, one PMP can be determined from each CMIP5 model. Collectively, the five estimates from the five CMIP5 models with more skillful simulations of atmospheric rivers provide us an ensemble of PMP estimates with uncertainty information indicated by the spread of the ensemble.

$$MP = p \cdot \frac{PWM(SST)}{PW(SST)} \tag{2}$$

In summary, our proposed hybrid approach differs from the HMR57 approach in the following ways. (1) Our approach relaxes several assumptions in the HMR57, which makes it more physical. This includes the possibility of air parcel to move vertically in the back trajectory procedure, and the search of maximum moisture maximization ratio (along the whole back trajectory track) rather than a given time point (i.e., the end point of the back trajectory that ends at the start time of the storm starting time in HMR57). (2) By analyzing climate model data, we search for more extreme events than those considered in HMR57. The large enough selection of the local extreme events also allows our approach to avoid the storm separation and orographic adjustment. (3) Our approach takes the precipitation information at the whole upstream watershed, so those depth-area-duration curves can be reduced to the duration-depth relationship. These improvements make the approach more objective.

2.4. Sensitivity of PMP to Climate Change

If we rewrite equation (1) as

$$PMP = \frac{p}{PW} \cdot PWM \tag{3}$$

PMP is affected by two factors: PWM that reflects the maximum moisture availability, and the ratio p/PW that reflects the capability of the storm to convert precipitable water to precipitation, which we call "storm efficiency" in this study. This efficiency has been investigated by Kunkel et al. (2013b), and it is closely related to the atmospheric vertical velocity that produces adiabatic cooling of the air mass and condensation of the water vapor to clouds. During extreme precipitation events, moisture several times larger than the precipitable water can be converted to actual precipitation over the storm life cycle (Kunkel et al., 2013b).

Constrained by the energy balance, large-scale atmospheric overturning circulations will slow down with warming (Held & Soden, 2006), which will manifest in reduced vertical velocity in the tropical circulations. However, in the mid and high latitude, changes in vertical velocity were found to be generally small (Kunkel et al., 2013b). In the extratropics, changes in the storm tracks are more likely to influence extreme precipitation (Lu et al., 2014; Pfahl et al., 2017). Changes in moisture tracks have impacts on PW and PWM, which modify the PMP. Consider the ratio of $PWM(SST)/PW(SST)$ in equation (2) to be a function of SST, the change in PMP in the future can be written as the sum of changes due to two factors related to the change in the back trajectory endpoint and the warming at that location that jointly determine the SST at the endpoint. Therefore, SST warming (thermodynamical effect) and moisture track change (dynamical effect) is another pair of competing factors that determine PMP changes in the future.

Given the availability of climate projection in the future period, four experiments are designed to understand the sensitivity of PMP to the two pairs of factors (PWM versus p/PW changes and warming versus

Table 2
Design of the Four Experiments

Code	Simulation period	Precipitation (p)	SST in the event (t)	Maximum SST (m)
p0t0m0	1970–2016	Historical	Historical	Historical
p0t0m1	1970–2016	Historical	Historical	Future
p1t1m1	2050–2099	Future	Future	Future
p10t10m10	2050–2099	Future but quantile-mapped to historical values	Future but quantile-mapped to historical values	Future but quantile-mapped to historical values[a]

[a]This value is identical to historical maximum SST (since they share the same quantile of 100% in the statistics).

moisture track change) of climate change. The configurations of these experiments are shown in Table 2. Experiment p0t0m0 performs back trajectory using historical climate simulations to generate PMP estimations for the historical period (1970–2016). Experiment p0t0m1 is the same as p0t0m0 except that the future maximum SST (i.e., maximum moisture availability) at the end point of the historical back trajectory is used to maximize the precipitation. Hence, the difference between p0t0m1 and p0t0m0 reflects how the projected changes in maximum moisture availability would affect PMP. Experiment p1t1m1 estimates the PMP using climate simulations for the future period of 2050–2099. The increased value of PMP from p0t0m0 to p1t1m1 provides an estimation of the changes in PMP between the future and historical periods. Lastly, experiment p10t10m10 is designed to study the impact of moisture track shift under future climate change on PMP. In this experiment, back trajectory is performed using the future simulation, but the precipitation amount and SST of the future period are both quantile-mapped to the historical values. Here quantile-mapping is used in this procedure. Using precipitation as an example, the exceedance frequency of a given future event is determined from the future ~~3 day~~ precipitation Cumulative Distribution Function (CDF) curve. This frequency is then used to determine the corresponding ~~3 day~~ precipitation amount based on the historical CDF curve. Since SST determines *PW* and *PWM*, all quantities used to estimate PMP in this experiment reflect the historical thermodynamic environment, so the difference between p0t0m0 and p10t10m10 reflects the changes of moisture track that alter the end point of the back trajectory in the future climate simulations relative to the historical climate simulations. The relationship of the four PMP estimations is also illustrated in Figure 3.

2.5. Robust Uncertainty Estimation

Previous studies suggest that a minimum of 8–10 climate models are required to make a robust estimate on the uncertainty of a climate variable (Mote et al., 2011). Here we use 10 models in total to derive more robust uncertainty estimates.

First is the adjustment of the ensemble. As shown in supporting information Figures S1 and S2, the mean of maximum ~~3 day~~ precipitation and the moisture maximization ratio are almost the same between the 5-model ensemble and the 10-model ensemble. Therefore, the ensemble mean estimation of PMP does not require adjustment.

Then the uncertainty can be estimated for each step of the PMP estimation, following an approach proposed in Micovic et al. (2015). By dividing the total uncertainty into uncertainty within the maximum ~~3 day~~ precipitation and within the maximization ratio, the variation of the 10-model ensemble PMP, i.e., Var10(PMP), can be approximated using equation (4).

$$Var10(PMP) = Var5(PMP) \times \frac{Var10\ (\mathrm{max\_3}day\_P)}{Var5\ (\mathrm{max\_3}day\_P)} \times \frac{Var10\ (\mathrm{maximization\_ratio})}{Var5\ (\mathrm{maximization\_ratio})} \tag{4}$$

where Var5(X) is the standard deviation of X based on the 5-model ensemble and Var10(X) is the standard deviation of X based on the 10-model ensemble.

The moisture maximization ratio is taken as the average ratio in the ocean region within 15°N–55°N and from 180°W to the U.S. west coast. In estimating the maximization ratio, it is necessary to define an "event PW." This event PW is estimated using the X% exceedance frequency SST. Since most of the extreme precipitation events in the PNW happen in winter, we vary X between 0 and 50, and it turns out that the maximum *Var10* (*maximization ration*)/*Var5* (*maximization*) is about 1.1 (supporting information Figure S3).

AGU Water Resources Research 10.1002/2017WR021094

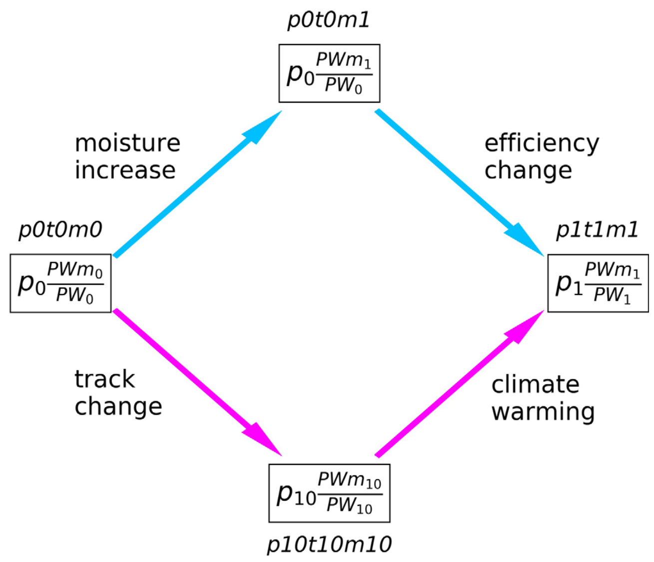

Figure 3. Relationship among the four PMP estimates in the experiments. The left PMP estimation (p0t0m0) uses all the historical information (historical PMP); the rightmost PMP estimation uses all the future information (future PMP); the top PMP estimation differs from the historical PMP only in the change of maximum moisture availability due to SST warming; the bottom PMP estimation reflects only the changes in the moisture track of extreme storms relative to the historical PMP. From these experiments, the difference between historical and future PMP can be decomposed into: moisture change and storm efficiency change (the blue pathway); or moisture track change and atmospheric warming (the magenta pathway).

Therefore, 110% is used in equation (4) to extend the uncertainty in the maximization ratio obtained from the 5-model ensemble.

3. Results

3.1. Simulation Skill in CMIP5

Extreme storms in the PNW region are strongly influenced by atmospheric river (AR) events (Leung & Qian, 2009). Consistently, ARs accounted for most of the flooding events in Washington State (Neiman et al., 2011). Thus, it is important that the climate models used in the PMP estimation skillfully simulate the AR climatology. Figure 4 shows the simulated AR days over the PNW from 24 CMIP5 models as gray lines, as well as the mean of four reanalysis products (CFSR, ERA-Interim, MERRA, and NCEP1) as black line, as analyzed by Gao et al. (2015). Here AR days refer to the number of days with an AR detected along the PNW coast (40°N–50°N). It is clear that ARs make landfall in the PNW coast more frequently in fall and winter. All 24 CMIP5 models have realistic seasonality, but some of them fail to capture the increased AR days from fall to winter. Based on this evaluation, five CMIP5 models that can best capture the AR days climatology (red lines) are selected for PMP estimations in this study. The blue lines show the performance of the five additional models for PMP uncertainty check, and most of them also exhibit the similar trend of AR days in autumn and winter.

3.2. Historical PMP Estimation

Since we combined the traditional engineering practice with climate model data, it is useful to compare the hybrid PMP estimation with the established PMP values to determine a common baseline. Figure 5 shows the sites of the established PMP values in HMR 57 (red dots), as well as their upstream watersheds as derived from river network database (Wu et al., 2012). We applied this hybrid approach to each HMR57 watershed to derive the PMP for that watershed. Thus, it carries the same upstream drainage area as the HMR57 design values. Figure 6 compares the HMR PMP values to the hybrid PMP values estimated using data from each CMIP5 model (Figures 6a–6e), as well as the multimodel ensemble (MME) mean historical estimation based on the five models (Figure 6f).

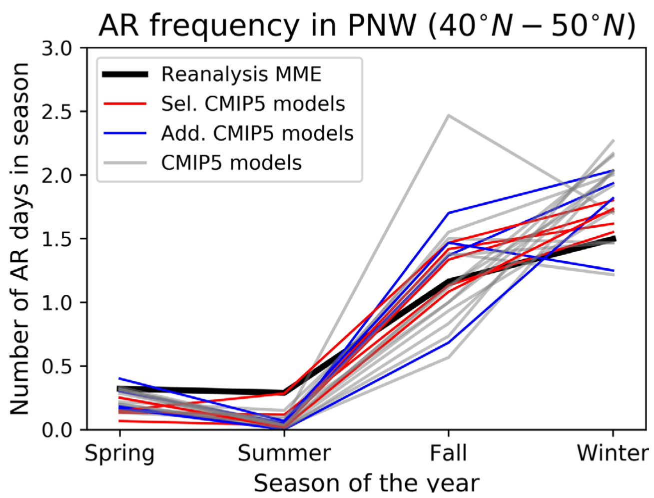

Figure 4. Comparison of CMIP5 simulated atmospheric river (AR) climatology defined as the number of AR days over PNW with reanalysis data. Black line shows the mean of four reanalysis products (CFSR, ERA-Interim, MERRA, and NCEP1), red lines show the AR frequency in five CMIP5 models used for PMP estimation (ACCESS1-0, CMCC-CM, CNRM-CM5, GFDL-ESM2G, and MPI-ESM-LR), and blue lines are the AR statistics from five additional CMIP5 models for uncertainty estimation (ACCESS1–3, CanESM2, HadGEM2-CC, HadGEM2-ES, and MIROC5). Gray lines show the AR statistics from all the 22 evaluated CMIP5 models. Data are taken from Gao et al. (2015).

Regarding the PMP values, the performance among the five models varies, from heavy underestimation in CMCC-CM to slight overestimation in MPI-ESM-LR. The five models can be classified into three groups: (1) CMCC-CM, which underestimates PMPs in all evaluation watersheds; (2) CNRM-CM5, ACCESS1-0, and GFDL-ESM2G, which provide consistent estimates as HMR, with slightly underestimated PMPs in certain basins; (3) MPI-ESM-LR, which slightly overestimates PMPs than HMR. Despite this variation, all five models correctly reproduce the spatial heterogeneity and the magnitude of PMP with the lowest correlation coefficient of 0.67, which is acceptable given the range of available HMR PMPs (between 150 and 900 mm) and the varying sizes of the upstream watersheds (between ~~9 and 10,900 mi^2~~) in the domain. The MME mean still tends to underestimate PMPs, but the HMR values fall within the envelope of the MME range in most watersheds (Figure 5f). The variation of MME increases as the PMPs become larger, which suggests increased variations in the extreme precipitation simulation in the models. It is also interesting to see that the

ID: kannanb Time: 13:55 I Path: //chenas03/Cenpro/ApplicationFiles/Journals/Wiley/WRCR/Vol00000/170508/Comp/APPFile/JW-WRCR170508

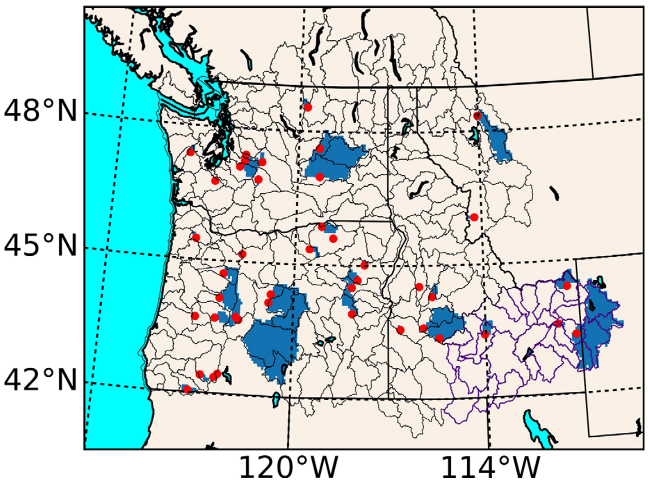

Figure 5. Locations of the 43 PMP estimation sites in the Hydro-Meteorological Report (HMR) 57. Red dots denote the locations of dams/reservoirs, and blue areas are the upstream watersheds of these sites. The background is the Hydrological Unit (HU8) watersheds in the PNW region. Upstream watersheds are derived using the river network database in Wu et al. (2012).

simulated PMP does not always benefit from the use of finer resolution climate model data; with the finest atmospheric grid size among the five models, CMCC-CM produces the most biased results. Since we used the LOCA-downscaled precipitation, biases in the GCM precipitation are inherently removed so the effects of model resolution on precipitation are minimized. Differences in the hybrid PMP skill among the models are likely related to model biases in the moisture tracks and SST relative to the observations, which are not expected to have a simple relationship with the model grid sizes.

Reanalysis product is a bridge between observation and climate simulations, as they are often used to evaluate the various climate simulations (Sheffield et al., 2013). Therefore, along with these five CMIP5 models, we also did an experiment using the same hybrid approach, but with all the data from observation (i.e., Livneh precipitation, NOAA OISST SST) and reanalysis product (i.e., ~~6 h~~ ERA-Interim wind fields). As shown later, the observation/reanalysis-based estimation shows better spatial correlation than the CMIP5-based estimates here. The observation/reanalysis-based results are shown and discussed in details in section 4.2.

Figure 7 presents the geographic distribution of the hybrid PMP estimation. All five models show much higher PMP in the coastal region and a dramatic drop east of the Cascade Range. The PMP increases further east in the northern Rocky mountain range. This spatial pattern reflects the spatial variations of storm efficiency as influenced by topography and the spatial variations of

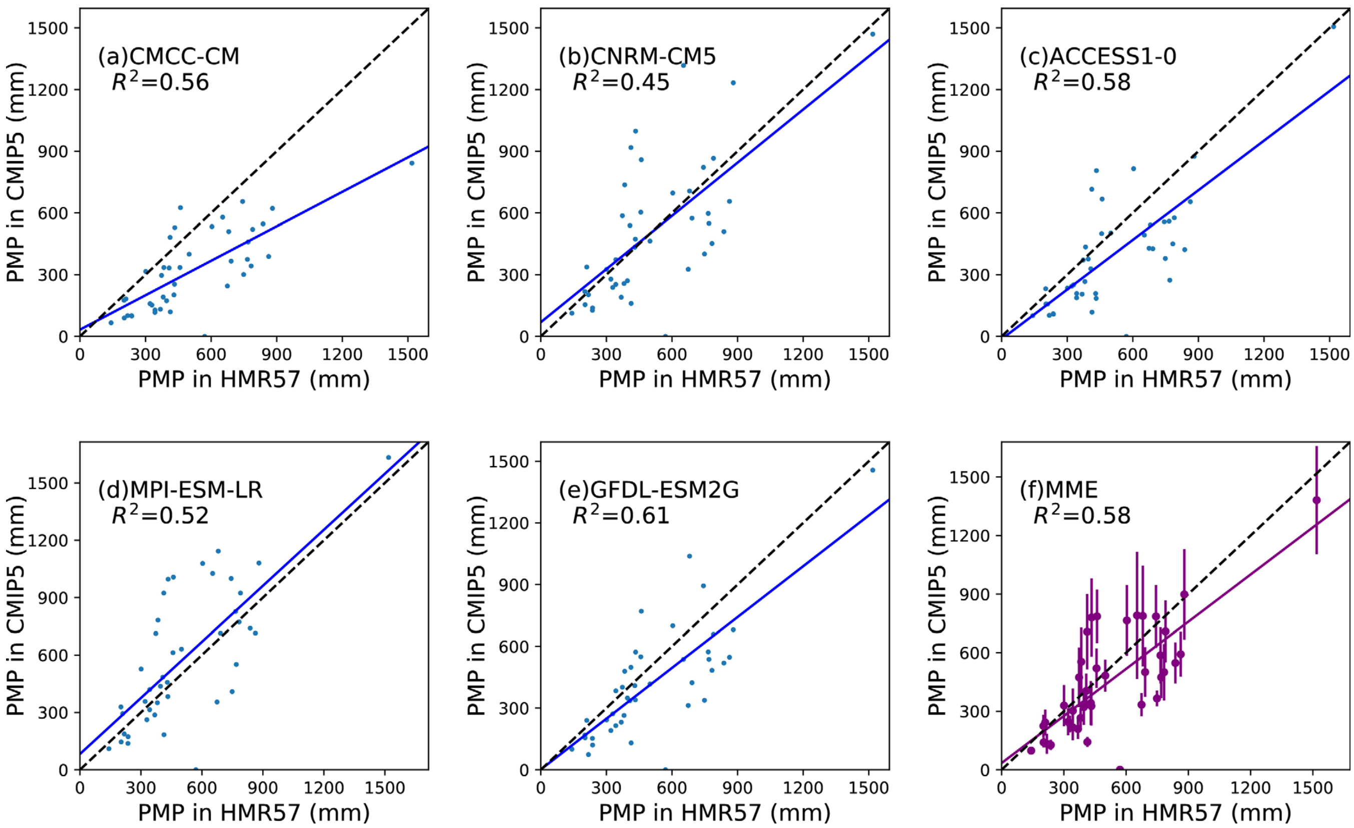

Figure 6. Evaluation of the hybrid historical PMP estimation against established values in HMR. The HMR PMPs are taken from basins shown as the red dots in Figure 1 and compared to the hybrid estimation. (a–e) The PMP estimates from individual CMIP5 models and (f) the ensemble mean and standard deviation of PMP estimation in the basins. Blue lines are the regression between HMR PMP and hybrid PMPs.

AGU Water Resources Research 10.1002/2017WR021094

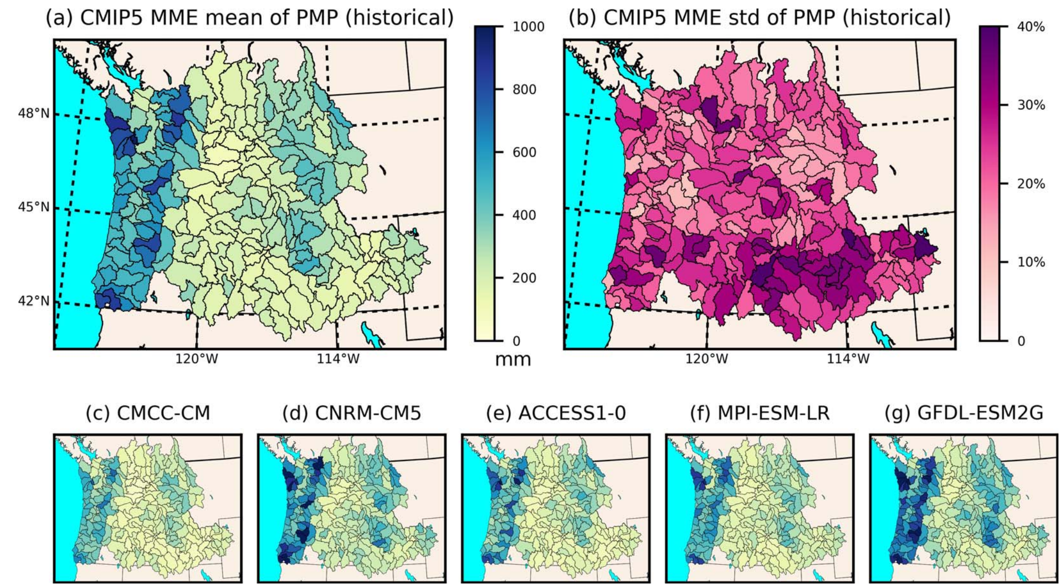

Figure 7. Hybrid PMP estimation from five selected CMIP5 models. (a) The multimodel ensemble mean PMP estimation using CMIP5 data for 1970–2016 and (b) the standard deviation (as percentage of the mean) among five models. (c–g) The PMP estimations from five individual models.

the moisture source regions. The spatial pattern of PMP is most significant in CNRM-CM5 and GFDL-ESM2G, and least significant in CMCC-CM, which is reflected in the regression in Figure 6. The uncertainty (i.e., standard deviation) of the hybrid PMP does not display strong spatial patterns (Figure 7b), and overall the standard deviation is about 20% of the MME mean. However, larger disagreement among different models is found in the southeast region of PNW, but PMP values are very small in that region.

3.3. PMP Change With Climate Warming

3.3.1. Total Change of PMP

Figure 8 compares the PMP estimations between the historical period (1970–2016) and future period (2050–2099), from the two experiments p0t0m0 and p1t1m1, respectively. PMP increases in all PNW watersheds by up to 500 mm or 100% (Figure 8). The absolute change in PMP is largest in watersheds in the coastal range and Cascades range that already experiences more severe precipitation climatologically

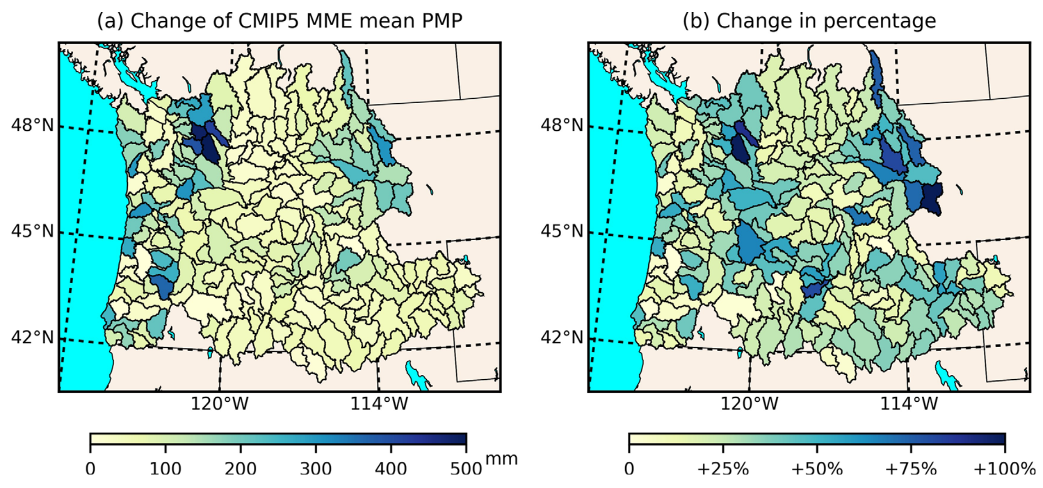

Figure 8. Changes of PMP by 2099 compared to PMP by 2016. (a) The amount of change in mm and (b) the change as percentage of historical PMP (1970–2016).

AGU Water Resources Research 10.1002/2017WR021094

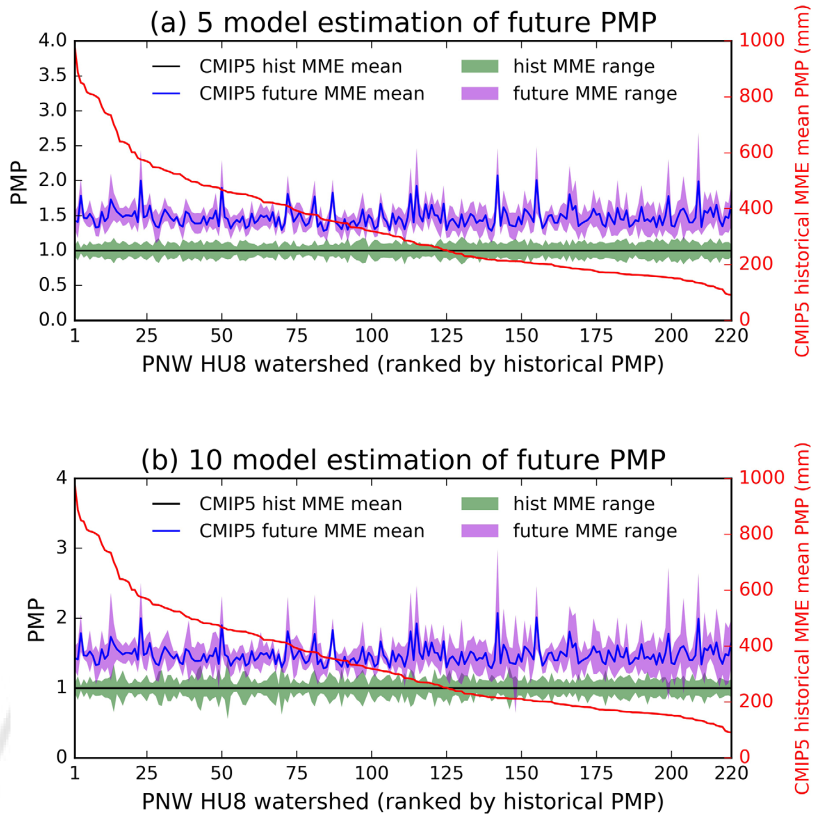

Figure 9. Historical (by 2016) and future (by 2099) PMP in PNW from CMIP5 ensemble estimation. (a) The uncertainty from 5-model estimation and (b) the results from 10-model estimation. Black lines are the historical multimodel ensemble (MME) historical mean PMP, and blue lines are the future mean PMP. Green and magenta ranges are the standard deviation in the MME estimation for historical and future period, respectively. All the data are normalized by the historical MME mean values (left *y* axis). After the normalization, all historical MME mean is equal to one (black line). The actual values of the historical MME mean are shown in the red line (right *y* axis). The *x* axis shows the 220 HU8 basins, which are arranged by their historical MME mean PMP with decreasing PMP values from left to right.

(Figure 7a). Percentage wise, the increase in PMP is more homogeneous across the watersheds, with an overall increase of about 50%.

To appreciate the significance of the PMP increase in the future, Figure 9 shows the 220 hydrological units in the domain along the *x* axis, arranged by their historical MME mean PMP from high values to low values (red line). The PMP values indicated by the *y* axis on the left-hand side of the figure are all normalized by the historical 5-model MME mean PMP (which is the same as the 10-model MME mean, as demonstrated in section 2.5), and the green envelope shows the range (defined as standard deviation) of MME estimates in the historical period. The blue line and magenta envelope show the MME mean and the range (defined as standard deviation) of PMP in the future. Figure 9a shows the uncertainty from the 5-model ensemble, and Figure 9b shows the 10-model ensemble results. For most watersheds, the future MME mean PMP is well outside the ensemble range of the historical MME, and vice versa, so the increase depicted in Figure 7 is significant. On average, the future MME mean PMP has an increase of about 50% over the historical MME mean across the domain, but in several watersheds the future PMP can increase by as high as 100% of the historical PMP. There is a tendency for the relative uncertainty (range) to increase from wet watersheds (basins on the left side of the *x* axis) to the dry watersheds (basins on the right side of the *x* axis). In absolute terms, the uncertainty (range) still decreases from wet watersheds to the dry watersheds.

3.3.2. Sensitivity of PMP to Climate Factors

Two sensitivity experiments (p0t0m1 and p10t10m10) were designed to examine the impact of individual climate change factor on the PMP change. As described in the method section, the total change of PMP can be either broken into available moisture change and storm efficiency change, or storm track change (dynamical effect) and warming (thermodynamical effect). Figure 10 shows the relative contribution of

AGU Water Resources Research 10.1002/2017WR021094

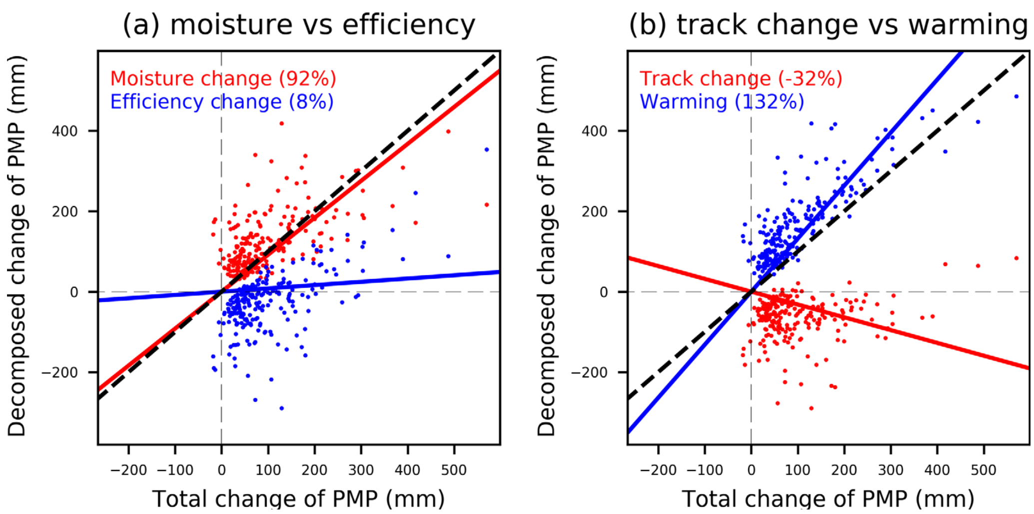

Figure 10. Changes of PMP corresponding to each contributing factor. (a) Breaks down the total change into changes due to moisture availability and changes due to storm efficiency change. (b) Breaks down the total changes into changes due to storm track shift and changes due to warming.

these factors. From Figure 10a, the increase of maximum moisture availability due to warming explains 92% of the total increase in PMP, while the storm efficiency increase is responsible for the rest or 8% of the increase. As illustrated in Figure 10a, changes in storm efficiency lead to a decrease of PMP in some basins. This negative contribution of storm efficiency change is consistent with the earlier finding that storm efficiency would decrease in a warming climate due to increase in atmospheric stability (Pauluis, 2015). However, if the increase of moisture can offset the decrease in the storm efficiency, the future PMP will still increase relative to current estimates. Figure 10b shows that atmospheric warming accounts for over 132% of the total PMP change, while moisture track shift has a contribution of −32% to the PMP increase. The latter result is consistent with Warner et al. (2015) and Gao et al. (2015), who found that changes in AR frequency and moisture transport in the North Pacific ARs are dominated by changes in atmospheric moisture associated with warming in the future. Also, Gao et al. (2015) found that changes in moisture pathways counter the increase in AR days due to warming, and our results also show opposite contributions of moisture track change and warming to PMP increase in the future.

Figure 11 shows the spatial distribution of the relative contributions of the four factors to PMP changes in the future. Both moisture availability and storm efficiency have a domain-wide impact, although moisture is more dominant. Comparing Figure 8b with Figures 11a and 11b, watersheds with an above-average percentage increase in PMP tend to be where storm efficiency plays positive roles in PMP changes. Notably, watersheds showing increased (decreased) contribution from storm efficiency are mostly located on the lee (windward) side of mountain ranges. This coincides with the findings that orographic precipitation tends to shift downwind in response to surface warming due to an upward shift of condensation with warming (Siler & Roe, 2014). Since LOCA provides spatial downscaling of precipitation through the use of historical analog, it can capture some effects of orographic adjustment but the extent to which it can represent changes in orographic precipitation in response to dynamical and thermodynamical changes in the atmosphere is not clear. Hence, the mechanisms for the changes in precipitation spatial distribution deserve further investigation in the future. Figures 11c and 11d show the partitioning of PMP changes contributed by storm track shift and warming, respectively. Warming plays a clear dominant role, and storm track shift results in noticeable positive changes in only a small number of watersheds. Interestingly, watersheds that have larger contributions from moisture track shift (Figure 11c) tend to also exhibit larger contributions from storm efficiency (Figure 11b). A possible explanation for these coincidental changes is that wind direction changes related to moisture track shift have an influence on orographically induced upward and downward motions, and hence storm efficiency. For example, several of the watersheds with notable positive contributions from moisture track shift and storm efficiency change are located on the lee side of the Cascade Range where changes from westerly to southwesterly winds may increase storm efficiency.

J_ID: **WRCR** Customer A_ID: **WRCR22987** Cadmus Art: **WRCR22987** Ed. Ref. No.: **2017WR021094** Date: **13-November-17** Stage: Page: **14**

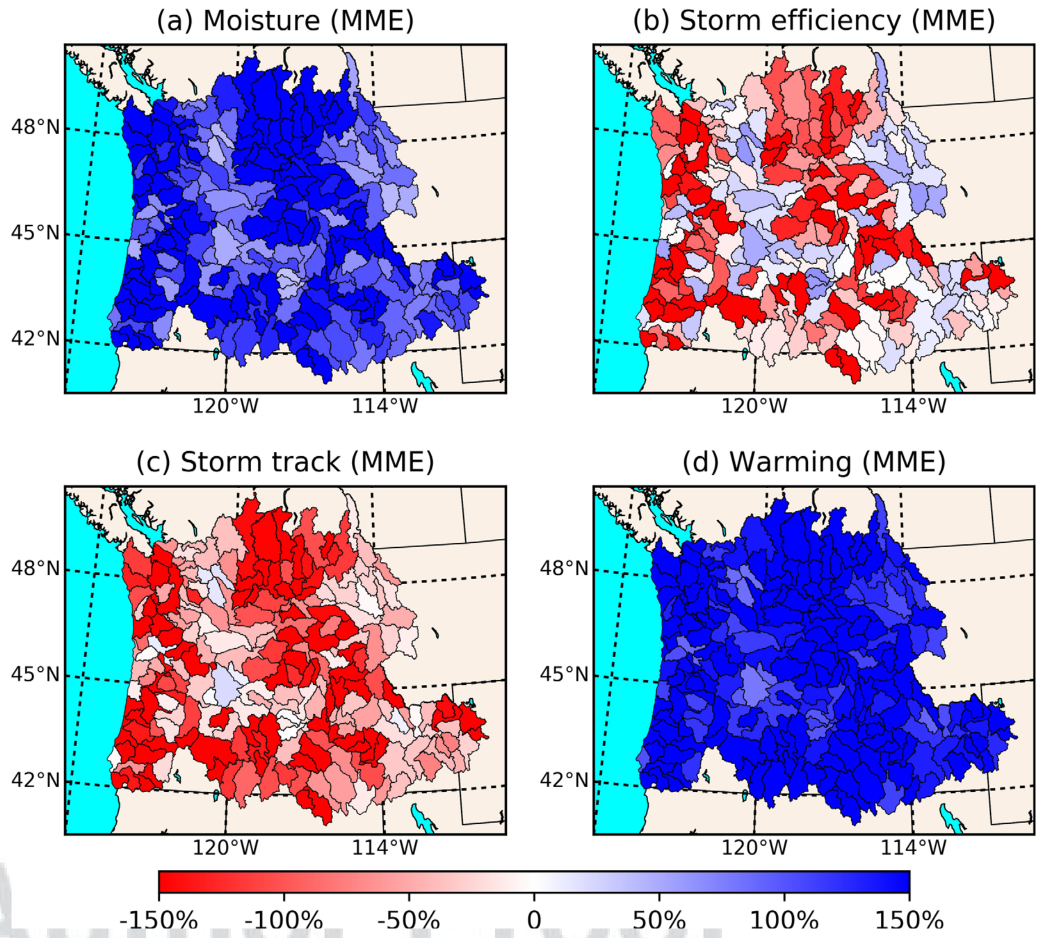

Figure 11. Contribution of different factors to the future change of PMP in the PNW. (a, b) The relative contribution (in percentage of total change of PMP) from increased moisture availability and increase storm efficiency. (c, d) The relative contribution from shifted storm track and atmospheric warming.

4. Discussion

4.1. Factors Affecting PMP Estimation Quality

As can be seen from equation (1), PMP based on the hybrid method is sensitive to the quality of the simulated precipitation and precipitable water and the SST field. Figures 6 and 7 show differing capabilities of CMIP5 models in capturing PMP in PNW. In this study, the differences in performance of the CMIP5 models in simulating precipitation may be reduced by the LOCA downscaling process, which includes bias correction and spatial downscaling.

SST data used in the PW estimation are obtained via back trajectory, so the first concern is the resolution of the climate models. Figures 6a–6e are arranged by the atmospheric model resolution, from 0.75° in CMCC-CM to 2° in GFDL-ESM2G. PMP estimation in CMCC-CM does not benefit from the higher resolution of atmospheric models, while GFDL-ESM2G is the within top two of the five models. Therefore, climate model resolution may not positively affect the PMP estimation results. This may be particularly true as one may expect larger impacts of model resolution on precipitation, but such impacts have been minimized by using statistically downscaled precipitation. On the other hand, previous studies showed that a minimum spatial resolution of about 12 km is needed to fully resolve the spatial characteristics of cold season extreme precipitation in mountainous regions, so the impact of model resolution may be more significant as we approach a much finer resolution (Prein et al., 2013).

Precipitation and SST also have a direct impact on the PMP estimation in equation (1). Since statistical downscaling method takes the same ground observation as a reference, the downscaled precipitation

ID: **kannanb** Time: 13:56 I Path: //chenas03/Cenpro/ApplicationFiles/Journals/Wiley/WRCR/Vol00000/170508/Comp/APPFile/JW-WRCR170508

Table 3
Evaluation of CMIP5 Simulated Daily SST

	Mean			std		Max		
Model	Corr	RMSE (K)	Bias (K)	Corr	RMSE (K)	Corr	RMSE (K)	Bias (K)
CMCC-CM	0.993	1.367	−0.53	0.907	0.464	0.980	2.716	−1.87
CNRM-CM5	0.995	0.862	−0.43	0.967	0.498	0.982	1.191	0.13
ACCESS1.0	0.995	0.922	−0.13	0.909	0.482	0.960	2.132	−1.18
MPI-ESM-LR	0.993	1.171	−0.49	0.918	0.438	0.980	2.101	−1.25
GFDL-ESM2G	0.994	1.538	−0.96	0.901	0.617	0.971	1.620	−0.37

Note: Evaluation is done in the 1982–2016 duration, with NOAA's OISST as reference. Bias is calculated as "model – OISST."

among climate models is made close to each other (via similarities to the reference data). The CMIP5 SST data are evaluated using NOAA's Optimum Interpolation SST data set (OISST; Banzon et al., 2016; Reynolds et al., 2007) for the overlapping period of 1982–2016, and the results are summarized in Table 3. The mean and variation are similar across the five models, but the construction of the maximum SST differs much more. It is important to point out that most of the extreme precipitation events in PNW occur in winter when SST is relatively cooler, so the SST during winter storms should be more characteristic of the PMP biases. Indeed, the bias (RMSE) of the constructed maximum SST also shares a lot of similarities with Figure 6, where CMCC-CM has the largest bias in the estimated PMP, and CNRM-CM5 has the least biases. This can be explained by the relationship between SST and PW used in practice (WMO, 1986): PW follows an approximately exponential relationship to SST, which heavily amplifies small biases in the maximum SST when SST is high. This, in turn, affects the maximization ratio, and therefore the final PMP estimation. As shown in Figure 10a, given all other factors (precipitation, representative SST of events) unaltered, the increase of maximum SST alone is responsible for 92% of the future PMP increase. This suggests that the impact of warming on PMP increase is most likely a response to the increases precipitable water, which is reflected as the increase of SST in the hybrid approach.

4.2. Evaluation of the Performance of Climate Model Output

Figure 12 shows the various experiments conducted using alternative data sources/approaches. Figure 12a uses the same hybrid approach, but with all the data from observation (i.e., Livneh precipitation, NOAA OISST SST) and reanalysis product (i.e., 6 h ERA-Interim wind fields). PMP is estimated using the available data during 1982–2013. This observation/reanalysis-based estimation shows better spatial correlation than the CMIP5-based estimations (Figure 6). However, the observation/reanalysis-based estimation tends to overestimate PMP. Since the reanalysis product is a reconstruction of historical climate, this overestimate can be explained by the slight differences in the back trajectory process: in the HMR57 instruction, the back trajectory is done along the surface, while in our hybrid approach the air parcel is allowed to move vertically. Thus, the trajectories might differ, leading to different "maximization location" (i.e., where the PWm(SST)/PW(SST) is found) identified.

Figure 12b shows a similar experiment, but with OISST replaced by PW from ERA-Interim to evaluate the impact of the SST-PW relationship (WMO, 1986) on the PMP estimation. It shows that as the SST-based PW is replaced with the reanalysis PW, the final PMP is heavily overestimated. Further investigation suggests that the reanalysis assimilated PW has a wider range (1–130 mm) than the SST-derived PW (8–123 mm). The similarity at the higher end (i.e., 130 mm versus 123 mm) indicates that the climatologically maximum precipitable water (PWm) from ERA-Interim is similar to those estimated from SST. However, the low end of precipitable water from ERA (around 1 mm) is significantly smaller than the SST-derived number (around 8 mm). As most of the extreme precipitation events in the PNW region happen in winter when SST and PW are low, this means that in Figure 12b, the lower PW numbers are often used to present the PW during the event. Such underestimation of the event PW then leads to the overestimation of PMP through equation (1).

Figure 12c shows the PMP estimation from a different approach using high-resolution climate simulation. The precipitation and PW data are taken from the 4 km WRF simulation during 2001–2012 (Liu et al., 2017), and the PMP estimation approach is taken from Rouhani and Leconte (2016). This approach leads to a more biased PMP estimation even using high-resolution dynamically downscaled data. Since the WRF simulation

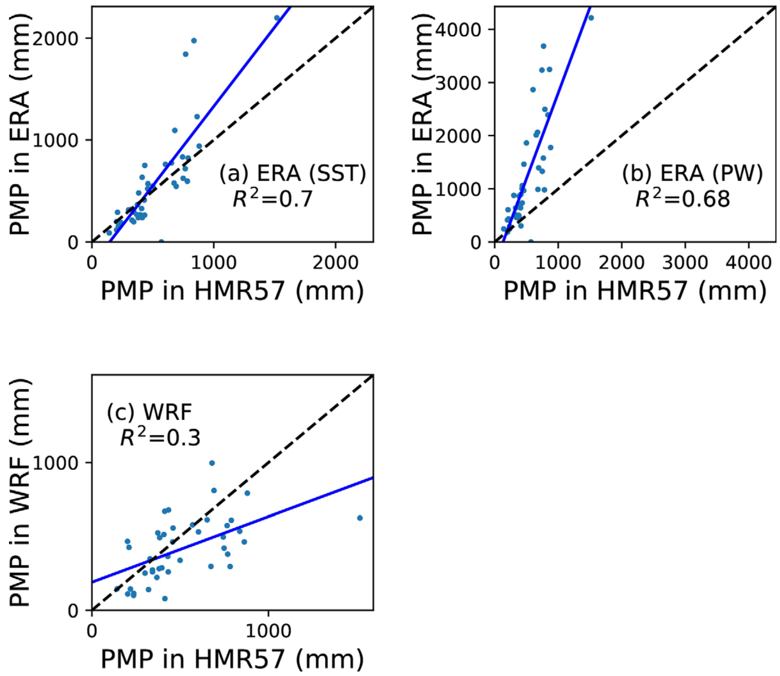

Figure 12. Historical ~~3 day~~ PMP estimation from alternative approaches. (a) Estimates PMP using the hybrid approach in this study, but with the 1982–2013 Livneh precipitation observation, ERA-Interim reanalysis winds, and SST observation. (b) Similar to Figure 12a, but with SST observation replaced by the precipitable water in ERA-Interim. (c) Estimates PMP using the approach proposed by Rouhani and Leconte (2016) and the 2001–2012 4 km WRF simulation of the continental U.S. (Liu et al., 2017). In all three figures, the *x* axis shows the PMP values in HMR 57, and the *y* axis shows the values from three alternative approaches.

is driven by ERA-Interim, the difference between Figures 12a and 12c suggests the impact of different methods as well as different data sources for the PMP estimation. It shows that back trajectory for PW search is necessary for the PNW region, which would help to keep the PMP estimation consistent with the HMR approach.

4.3. Impact of Bias in the Input Data on the Final PMP Estimation

The main source of bias in the hybrid approach is from the statistical downscaling of precipitation, as well as the SST data. Figure 13a compares the LOCA-downscaled maximum ~~3 day~~ precipitation against the PRISM gridded observation (Daly et al., 1994) across the 220 HU8 watersheds. In general, the extreme precipitation from LOCA exhibits good agreement with observation. If we divide the study region into three subregions: coastal/windward (Figure 13b), leeward (Figure 13c), and fareast of the PNW (Figure 13d), they show varied consistencies with good agreement in the windward and leeward regions but overestimation of extreme precipitation in the far-east region by LOCA. The overestimation in eastern PNW could be related to the coarse-resolution topography of CMIP5 models that allows more moisture to be transported across the Cascade Range to produce excess precipitation in the east. Apparently the LOCA bias correction is not able to fully account for the overestimation because bias correction mainly removes biases for the mean and variance rather than explicitly for extreme precipitation. Based on equation (1), this would lead to a higher estimate of PMP in the east part of the PNW region.

Another bias in statistically downscaling is from the stationarity assumption of bias correction and downscaling relationship. To check how much bias this introduces to the precipitation fields, the historical and future LOCA statistics are compared against dynamical downscaling (Figure 14). The dynamical downscaling in Figure 14 is produced by running WRF at 4 km resolution for 2001–2012 to construct historical climate, and perturbed boundary condition to construct 2070–2099 climate (Liu et al., 2017). Figure 14 indicates that under future warming, LOCA produces similar results as dynamical downscaling. Therefore, the nonstationarity within the LOCA methodology is not likely a big concern here.

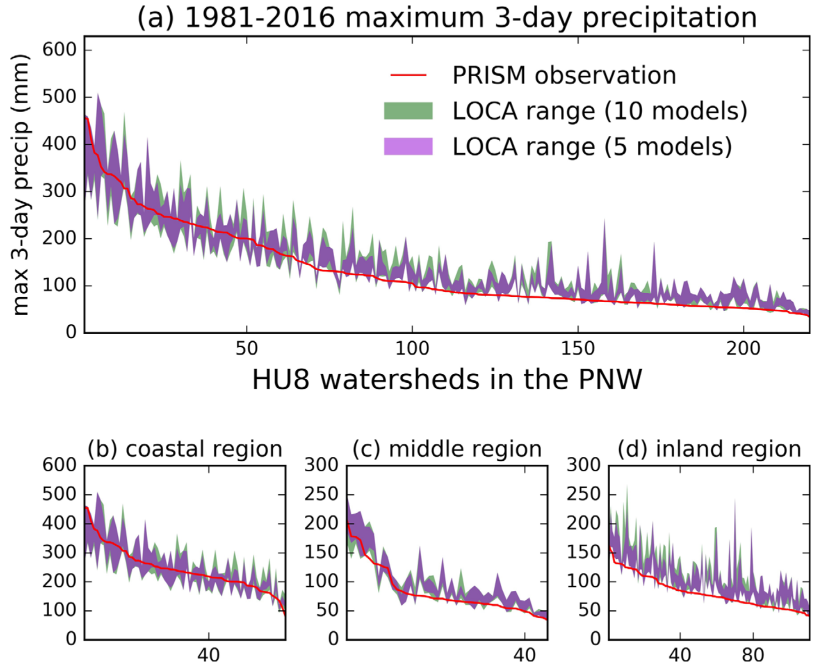

Figure 13. Evaluation of statistically downscaled maximum ~~3-day~~ precipitation in the PNW region. Here the LOCA-downscaled precipitation is compared against the PRISM gridded observation (Daly et al., 1994) in the 1982–2016 period. (a) The comparison at 220 Hydrological Unit (HU8) watersheds in the PNW and (b–d) the comparison of the coastal/windward watersheds, leeward watersheds, and watersheds in the eastern part of PNW. In all these figures, the *x* axis shows the HU8 watersheds arranged by PRISM maximum ~~3-day~~ precipitation and the *y* axis is the maximum ~~3-day~~ precipitation from PRISM (red lines) as well as the LOCA ranges in 5-model (magenta) and 10-model (green) ensembles.

Statistical downscaling techniques rely on ground observation, so the downscaled precipitation would also inherit the observational uncertainty (Henn et al., 2016). Since high-quality downscaled data provide precipitation that closely matches the reference observation, the uncertainty in the downscaled precipitation may exhibit similar uncertainty pattern as observation. In the PNW region, the observational uncertainty is larger over the Cascade Range region. Therefore, the observation-induced uncertainty may be worth considering in this area.

Biases in the SST is another potential source of bias to the PMP estimation, as any bias in SST would lead to amplified bias in PW and PWM through the nonlinear relationship between SST and moisture. Figure 15 compares the CMIP5 SST to the OISST observation in the 1982–2016 duration. Figure 15a compares the histogram of SST in the ocean regions between 15°N and 55°N, and 180°W and west coast. All of 10 models show similar histogram as observation. Given the low spatial variation of SST, such high consistency is expected. Figure 15b converts the SST to the PW using the relationship from WMO (1986), and the high consistency is still clear. Therefore, SST does not require extra bias corrections.

In summary, the PMP estimation in the PNW region is likely influenced by uncertainties from different sources: PMP in the eastern part of region is more affected by extra moisture penetration in the CMIP5 models, while PMP in the western part inherits more uncertainty from the observational uncertainty of precipitation. The evaluation here indicates that for the hybrid approach to work, high-quality precipitation is the top priority.

4.4. Usability of CMIP5 Output for PMP Estimation

The biggest disadvantage of directly using the CMIP5 output in PMP estimation is the coarse spatial resolution of data. This limits the models from correctly capturing mesoscale atmospheric systems such as hurricanes and local convective systems as well as orographic rainfall, so care should be taken when using those data sets. In the PNW region, most of the extreme precipitation is associated with AR events that are features of the large-scale atmospheric circulation. CMIP5 models have demonstrated their capability in capturing such systems (Figure 4; Gao et al., 2015; Lavers et al., 2013; Warner et al., 2015) so they are suitable for

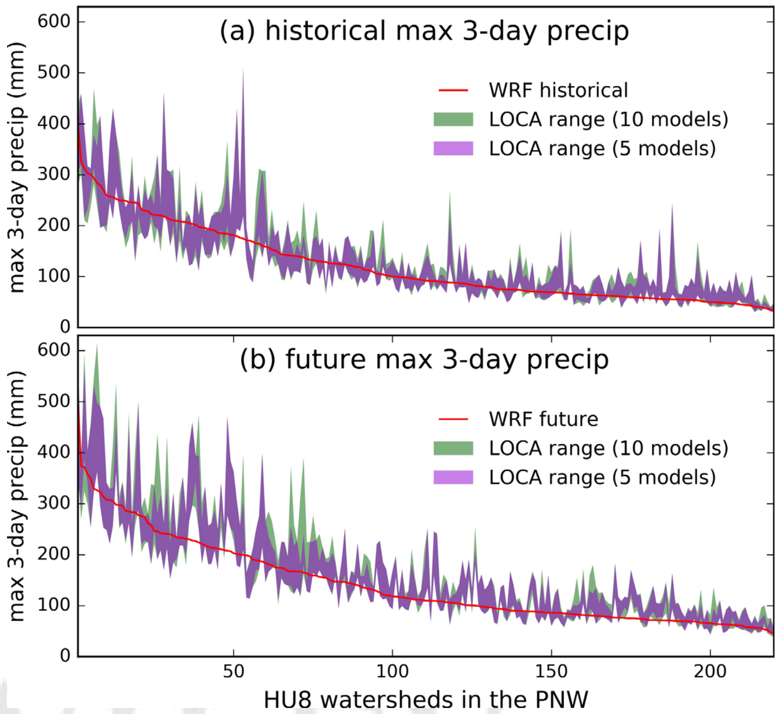

Figure 14. Evaluation of the nonstationarity in the LOCA-downscaled precipitation. Here the LOCA data are compared against the 4 km continental U.S. simulation for the (a) 2001–2012 period and (b) 2071–2099 period. The *x* axis is the Hydrological Unit (HU8) watershed, arranged by WRF maximum ~~3-day~~ precipitation. The *y* axis shows the max ~~3-day~~ precipitation in WRF (red lines), as well as the range of LOCA 5-model ensemble (magenta) and 10-model ensemble (green). 2001–2012 WRF simulation was driven by ERA-Interim reanalysis. 2091–2099 simulation was driven by modified ERA-Interim to reflect the climate in 2070–2099.

PMP studies in the PNW and other regions where extreme precipitation is dominated by AR events. As discussed above, the difference in climate model resolution has no significant impact on the final estimates, and SST itself has low spatial variation. Hence, the coarse-resolution precipitation data are the main limitation of CMIP5 particularly for the topographically diverse region of PNW. This issue, however, can be addressed using statistically downscaled high-resolution precipitation data that are readily available for the U.S. For PMP estimation in other regions where the moisture source for extreme precipitation may be more

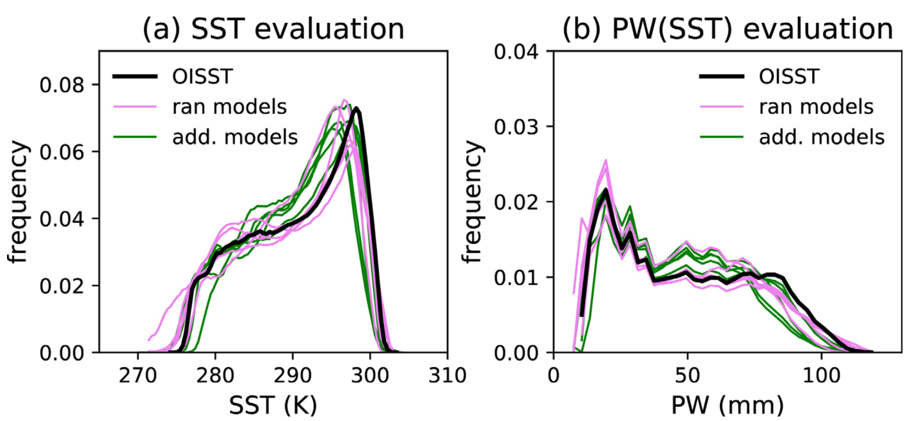

Figure 15. Evaluation of SST in the CMIP5 models. The evaluation area is the ocean area bounded between 15°N and 55°N and from 180°W to the PNW coast. (a) The histograms of SST in this region and (b) the precipitation as calculated from SST using the relationship in WMO (1986). In both figures, black lines are the histograms from NOAA's Optimum Interpolation SST (OISST) observation (Banzon et al., 2016; Reynolds et al., 2007), pink lines are from five CMIP5 models used for PMP estimation, and green lines are the five additional CMIP5 models for PMP uncertainty estimation.

local, high-resolution PW data may also be required. Recently developed methods such as the adaptable random forest method presented in He et al. (2016) provide promising venues for use with the hybrid approach before higher-resolution GCM or RCM outputs are available.

4.5. Trade-Off of Using Climate Models in PMP Estimation

Previous studies have used dynamically downscaled climate model data (Beauchamp et al., 2013; Rastogi et al., 2017; Rouhani & Leconte, 2016; Rousseau et al., 2014). Compared with these studies, our approach involves as much raw climate model output as possible, and we show that with the advance of computationally efficient techniques (such as statistical downscaling, and HYSPLIT), the raw model output can be quickly converted to ready-to-use data for the engineering communities. We demonstrate that combining the engineering practice with climate model data provides PMP estimates that are close to the ones used in the current engineering practice. This consistency provides confidence for using our PMP estimates for the future in safety evaluation. The method tested in this study inherits some familiar issues of traditional approach (mainly the linear assumption between PW and precipitation as criticized by Abbs (1999)). However, the hybrid method represents an important intermediate step in the transition of the current engineering approach to an entirely model-based approach. Most importantly, the hybrid method facilitates comparison with the traditional approach and allows biases to be evaluated and factors contributing to the future changes in PMP to be quantified and understood relative to what is already in use. Comparison of the hybrid approach with the full model-based approaches can reveal the influence of various storm maximization approaches used in the model by controlling the input data. Through this connection, a more reliable transition to full model-based PMP can be achieved.

In this study, PMP is estimated only through local storm maximization. In HMR57, big storms are also transposed from nearby regions (of similar climatology) to circumvent the limited or missing observational records to provide a broader collection of extreme events (e.g., rain gauge at the Nashville international airport stopped working during the Nashville 2010 May epic flooding; Chen et al., 2017). With climate models, long records of extreme precipitation (and other meteorological fields) are available, which (especially as an ensemble) allow us to investigate the climate signals of extreme precipitation, thus PMP in the future climate. The complete model output fields allow us to conduct more realistic estimation, e.g., by advancing back trajectory analysis of air mass along the surface to 3-D back trajectory as illustrated in this study. These advantages help fulfill the demands of storm transposition, as suggested by the similarities of PMPs in Figure 5.

4.6. How Likely Will the Historical PMP Be Surpassed in the Future?

Extreme precipitation is projected to change in a changing climate, but whether future storms will exceed the design standards of existing infrastructures remains a question. This is a safety issue beyond analysis of PMP changes: if the current PMP is going to be surpassed by future storms, a safety reevaluation is more urgent than that prompted by the finding that PMP will increase. Figure 16 shows the future max ~~3 day~~ precipitation as a percentage of the historical MME mean PMP. The MME range of future max ~~3 day~~ precipitation and historical PMP estimation is also shown in the figure. Historical PMP (black dashed line) is about 250% of the historical max ~~3 day~~ precipitation (solid black line). Future maximum ~~3 day~~ precipitation is around 45%–50% of the historical PMP. Thus, infrastructures will not encounter "PMP storms" under the future climate. Even when considering the uncertainties in both historical PMP (light green envelope) and future max ~~3 day~~ precipitation (magenta envelope), the risk of future extreme precipitation exceeding the historical design standards is still very low.

It is also worth pointing out that ~~3 day~~ PMP is associated with higher uncertainties than max ~~3 day~~ precipitation. According to our definition in equation (1), PMP inherits uncertainty in the max precipitation, which is then amplified by uncertainties in the moisture condition (PW and PWM). Figure 16 shows that standard deviation of maximum ~~3 day~~ precipitation is only about 20% of the MME mean, while Figure 9b indicates that the standard deviation of PMP can be as high as 40% of the MME mean. To further reduce the uncertainty of PMP estimation, more accurate precipitation data together with related meteorological fields (PW, temperature, and winds) are all needed.

4.7. On the PMF Estimation

The hybrid approach proposed in this study provides PMPs estimation for the critical large water management infrastructures. At the same time, a large amount of such infrastructures have been designed using

AGU Water Resources Research 10.1002/2017WR021094

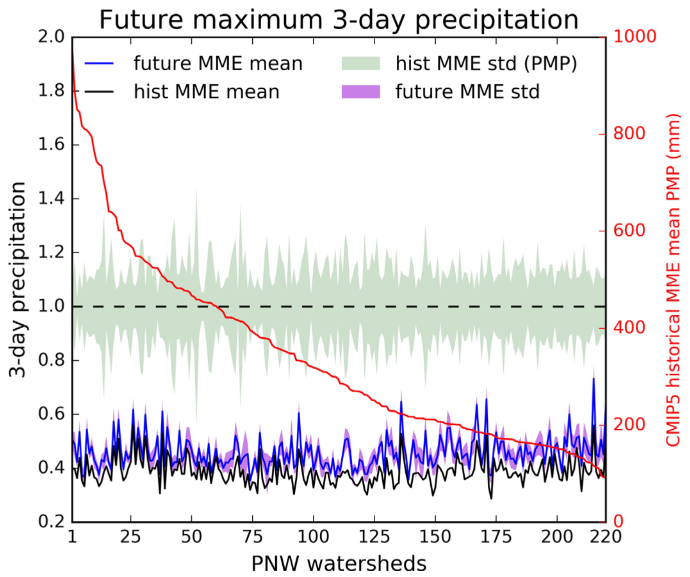

Figure 16. Maximum ~~3 day~~ precipitation as projected by CMIP5 models. The blue line is the 10-model MME mean, and the magenta envelope is the variation (defined as standard deviation) of MME. The solid black line is the 10-model MME mean of historical max ~~3 day~~ precipitation, and the black dashed line is the 10-model MME mean historical PMP. All the data are normalized by the historical MME mean PMP value (left *y* axis). The actual historical MME PMP is shown as the red line (right *y* axis). The light green envelope is the MME range of historical PMP. The *x* axis shows the 220 HU8 basins, which are arranged by their historical MME mean PMP.

probable maximum flood (PMF) criteria (Hossain et al., 2012). For the PMF estimation using this hybrid approach, the PMP storm is fed into the surface hydrological model, which would produce the streamflow timeseries at the watershed outlet. Since surface hydrological models generally require subdaily input, here is what the engineers should do to develop the PMP storm that can be used by these models (with the example of Grand Coulee dam location):

1. Delineate the upstream watershed boundary of the location (i.e., the location is the outlet of the delineated watershed).
2. Replace the daily precipitation data used here with subdaily data set. Some climate model output is available at subdaily time step, such as the MOAR run of CCSM4, which is available at 6 h resolution. Further downscaling these climate model data would provide suitable data for the hybrid approach.
3. Follow the instructions given in this study and compute the PMP of the watershed. Also at this point, we know which storm generates the PMP estimation as well as the maximization ratio.
4. Multiply the maximization ratio to all the subdaily precipitation maps (in the 72 h duration) of the storm identified in step 3. We now get the spatial-temporal information of the PMP storm that can be used in hydrological models. PMF can then be estimated.

Since different locations of storm center would impact the streamflow at the watershed outlet, in practice it may be best to check several PMP-class storms (i.e., those storms whose MP after maximization is close to PMP) so the worst streamflow process can be identified.

5. Conclusions

In this study, we applied a traditional PMP estimation approach (moisture maximization) to CMIP5 model outputs and estimated PMP over the PNW region. Model outputs from five CMIP5 models were used to assess PMP by 2016 and by 2099. The major conclusions are as follows:

1. Combining traditional PMP estimation approach with modern climate science and model data can provide PMP estimates that are consistent with the values used in current engineering practice.
2. In the worst climate scenario (RCP8.5), PMP in the PNW region is projected to increase by about 50% $\pm$ 30% by 2099 relative to current levels. This change is significant when considering the uncertainties of PMP estimation.
3. Most of the increase in PMP can be attributed to climate warming, which mainly affects moisture availability through the effects on SSTs. Future change of storm efficiency and storm track tend to reduce the future PMP.
4. PMP presents larger uncertainty than extreme precipitation. Thus, it is important to have high-quality data for both extreme precipitation and the related meteorological fields (3-D wind fields, temperature) for more accurate PMP estimation.

The hybrid approach presented in this paper connects the traditional PMP estimation and model-based approaches that are becoming popular recently. This study shows that selected climate model outputs are useful for PMP estimation in certain climatological regions such as the AR dominated PNW studied here, as they present similar quality as ground-based observation data after bias correction (such as the LOCA downscaling). Attributing the contributions of various processes to the PMP change in the future using the hybrid approach yielded results that are physical and consistent with previous findings regarding the effects of warming on storm efficiency and moisture tracks. This supports the physical basis of the hybrid approach through its adoption of physically and dynamically consistent climate model outputs and effective back trajectory analysis method. Although the method for the presented PNW case here can only be applied to other regions that also experience ARs, the idea behind the method is to use downscaled climate data together with traditional method for the PMP estimation. This would be applicable to all the locations

AGU Water Resources Research 10.1002/2017WR021094

where PMP estimation is needed. Future work may further take advantage of atmospheric models and global/regional climate model data to advance state of the art for PMP estimation in a changing climate.

Acknowledgments
We acknowledge the World Climate Research Programme's Working Group on Coupled Modelling, which is responsible for CMIP, and we thank the climate modeling groups (listed in Table 1 of this paper) for producing and making available their model output. For CMIP, the U.S. Department of Energy's Program for Climate Model Diagnosis and Intercomparison provides coordinating support and led the development of software infrastructure in partnership with the Global Organization for Earth System Science Portals. L.R. Leung was supported by the U.S. Department of Energy (DOE) Office of Science Biological and Environmental Research as part of the Regional and Global Climate Modeling program. PNNL is operated for DOE by Battelle Memorial Institute under contract DE-AC05–76RL01830.
AQ7 *Data policy*. All the data used in this study are publicly accessible. Specifically, 10 CMIP5 model output (SST, 3-D wind, air temperature, relative humidity, and geopotential height) is obtained through the Climate and Environmental Retrieval and Archive at the German Climate Computing Center (DKRZ; https://cera-www.dkrz.de/WDCC/ui/cerasearch/q?query=*%3A*&page = 0. Registration is required, which is free of charge). LOCA statistically downscaled data are part of the "Downscaled CMIP3 and CMIP5 Climate and Hydrology Projections" archive at ftp://gdo-dcp.ucllnl.org/pub/dcp/archive/cmip5/loca/LOCA_2016-04-02/. The 4 km WRF simulation data, which are described in Liu et al. (2017), can be accessed from NCAR's Research Data Archive (https://rda.ucar.edu/datasets/ds612.0/). HYSPLIT model (version 851) is obtained from NOAA's Air Resources Laboratory (http://ready.arl.noaa.gov/HYSPLIT.php, registration is required for Linux version). All the data used in this study (including the HYSPLIT format of CMIP5 input) are available upon request to first author.

APPROVED

References

Abbs, D. J. (1999). A numerical modeling study to investigate the assumptions used in the calculation of Probable Maximum Precipitation. *Water Resources Research*, *35*(3), 785–796. https://doi.org/10.1029/1998WR900013

Allan, R. P., & Soden, B. J. (2008). Atmospheric warming and the amplification of precipitation extremes. *Science*, *321*(5895), 1481–1484. https://doi.org/10.1126/science.1160787

Ashrafi, K., Shafiepour-Motlagh, M., Aslemand, A., & Ghader, S. (2014). Dust storm simulation over Iran using HYSPLIT. *Journal of Environmental Health Science and Engineering*, *12*(1), 9. https://doi.org/10.1186/2052-336X-12-9

Banzon, V., Smith, T. M., Chin, T. M., Liu, C., & Hankins, W. (2016). A long-term record of blended satellite and in situ sea-surface temperature for climate monitoring, modeling and environmental studies. *Earth System Science Data*, *8*(1), 165–176. https://doi.org/10.5194/essd-8-165-2016

Beauchamp, J., Leconte, R., Trudel, M., & Brissette, F. (2013). Estimation of the summer-fall PMP and PMF of a northern watershed under a changed climate. *Water Resources Research*, *49*, 3852–3862. https://doi.org/10.1002/wrcr.20336

Brimelow, J. C., & Reuter, G. W. (2005). Transport of atmospheric moisture during three extreme rainfall events over the Mackenzie River Basin. *Journal of Hydrometeorology*, *6*(2001), 423–440. https://doi.org/10.1175/JHM430.1

Casagli, N., Dapporto, S., Ibsen, M. L., Tofani, V., & Vannocci, P. (2006). Analysis of the landslide triggering mechanism during the storm of 20th-21st November 2000, in Northern Tuscany. *Landslides*, *3*(1), 13–21. https://doi.org/10.1007/s10346-005-0007-y

Chen, B., De Xu, X., Yang, S., & Zhang, W. (2012). On the origin and destination of atmospheric moisture and air mass over the Tibetan Plateau. *Theoretical and Applied Climatology*, *110*(3), 423–435. https://doi.org/10.1007/s00704-012-0641-y

Chen, B., Stein, A. F., Maldonado, P. G., Sanchez de la Campa, A. M., Gonzalez-Castanedo, Y., Castell, N., & de la Rosa, J. D. (2013). Size distribution and concentrations of heavy metals in atmospheric aerosols originating from industrial emissions as predicted by the HYSPLIT model. *Atmospheric Environment*, *71*, 234–244. https://doi.org/10.1016/j.atmosenv.2013.02.013

Chen, X., & Hossain, F. (2016). Revisiting extreme storms of the past 100 years for future safety of large water management infrastructures. *Earth's Future*, *4*(7), 306–322. https://doi.org/10.1002/2016EF000368

Chen, X., Hossain, F., & Leung, L. R. (2017). Establishing a numerical modeling framework for hydrologic engineering analyses of extreme storm events. *Journal of Hydrologic Engineering*, *22*(8), 4017016. https://doi.org/10.1061/(ASCE)HE.1943-5584.0001523

Cheng, L., & AghaKouchak, A. (2014). Nonstationary precipitation intensity-duration-frequency curves for infrastructure design in a changing climate. *Scientific Reports*, *4*, 7093. https://doi.org/10.1038/srep07093

Cheng, L., AghaKouchak, A., Gilleland, E., & Katz, R. W. (2014). Non-stationary extreme value analysis in a changing climate. *Climatic Change*, *127*(2), 353–369. https://doi.org/10.1007/s10584-014-1254-5

Cohen, M., Artz, R., Draxler, R., Miller, P., Poissant, L., Niemi, D., . . . McDonald, J. (2004). Modeling the atmospheric transport and deposition of mercury to the Great Lakes. *Environmental Research*, *95*, 247–265.

Daly, C., Neilson, R. P., & Phillips, D. L. (1994). A statistical-topographic model for mapping climatological precipitation over mountainous terrain. *Journal of Applied Meteorology*, *33*, 140–158. https://doi.org/10.1175/1520-0450(1994)033<0140:ASTMFM>2.0.CO;2

Dettinger, M. (2011). Climate change, atmospheric rivers, and floods in California—A multimodel analysis of storm frequency and magnitude changes. *Journal of the American Water Resources Association*, *47*(3), 514–523. https://doi.org/10.1111/j.1752-1688.2011.00546.x

Draxler, R. R., & Hess, G. D. (1997). *Description of the HYSPLIT4 modeling system*. Silver Spring, MD: U.S. Department of Commerce.

Draxler, R. R., & Hess, G. D. (1998). An overview of the HYSPLIT_4 modelling system for trajectories, dispersion, and deposition. *Australian Meteorological Magazine*, *47*, 295–308.

Draxler, R. R., & Rolph, G. D. (2012). Evaluation of the Transfer Coefficient Matrix (TCM) approach to model the atmospheric radionuclide air concentrations from Fukushima. *Journal of Geophysical Research*, *117*, D05107. https://doi.org/10.1029/2011JD017205

Evans, J. E., Mackey, S. D., Gottgens, J. F., & Gill, W. M. (2000). Lessons from a dam failure. *The Ohio Journal of Science*, *100*(5), 121–131.

Gao, M., Mo, D., & Wu, X. (2016). Nonstationary modeling of extreme precipitation in China. *Atmospheric Research*, *182*, 1–9. https://doi.org/10.1016/j.atmosres.2016.07.014

Gao, Y., Lu, J., Leung, L. R., Yang, Q., Hagos, S., & Qian, Y. (2015). Dynamical and thermodynamical modulations on future changes of landfalling atmospheric rivers over western North America. *Geophysical Research Letters*, *42*, 7179–7186. https://doi.org/10.1002/2015GL065435

Graziani, G., Klug, W., & Mosca, S. (1998). *Real-time long-range dispersion model evaluation of the ETEX first release*. Luxembourg: European Commission Joint Research Centre.

He, X., Chaney, N. W., Schleiss, M., & Sheffield, J. (2016). Spatial downscaling of precipitation using adaptable random forests. *Water Resources Research*, *52*, 8217–8237. https://doi.org/10.1002/2016WR019034

Held, I. M., & Soden, B. J. (2006). Robust responses of the hydrological cycle to global warming. *Journal of Climate*, *19*(21), 5686–5699. https://doi.org/10.1175/JCLI3990.1

Henn, B., Clark, M. P., Kavetski, D., Newman, A. J., Hughes, M., McGurk, B., & Lundquist, J. D. (2016). Spatiotemporal patterns of precipitation inferred from streamflow observations across the Sierra Nevada mountain range. *Journal of Hydrology*. https://doi.org/10.1016/j.jhydrol.2016.08.009~~, in press~~. AQ4

Hershfield, D. M. (1965). Method for estimating probable maximum rainfall. *Journal of the American Water Works Association*, *57*(8), 965–972.

Hossain, F., Degu, A. M., Yigzaw, W., Burian, S., Niyogi, D., Shepherd, J. M., & Pielke, R. Sr. (2012). Climate feedback-based provisions for dam design, operations, and water management in the 21st century. *Journal of Hydrologic Engineering*, *17*, 837–850. https://doi.org/10.1061/(ASCE)HE.1943-5584.0000541

Huang, Y., & Cui, X. (2015). Moisture sources of an extreme precipitation event in Sichuan, China, based on the Lagrangian method. *Atmospheric Science Letters*, *16*(2), 177–183. https://doi.org/10.1002/asl2.562

Ishida, K., Kavvas, M. L., Asce, F., Jang, S., Chen, Z., Asce, A. M., . . . Asce, A. M. (2015). Physically based estimation of maximum precipitation over three watersheds in Northern California: Atmospheric boundary condition shifting. *Journal of Hydrologic Engineering*, *20*(4), https://doi.org/10.1061/(ASCE)HE.1943-5584.0001026

Kunkel, K. E., Karl, T. R., Brooks, H., Bosart, L., Changnon, D., Cutter, S. L., . . . Wuebbles, D. (2013a). Monitoring and understanding trends in extreme storms: State of knowledge. *Bulletin of the American Meteorological Society*, *94*(4), 499–514. https://doi.org/10.1175/BAMS-D-11-00262.1

AGU Water Resources Research 10.1002/2017WR021094

Kunkel, K. E., Karl, T. R., Easterling, D. R., Redmond, K., Young, J., Yin, X., & Hennon, P. (2013b). Probable Maximum Precipitation and climate change. *Geophysical Research Letters*, *40*, 1402–1408. https://doi.org/10.1002/grl.50334

Lane, N. (2013). *Aging infrastructure: Dam safety*. Washington, DC: Congressional Research Service.

Lavers, D. A., Allan, R. P., Villarini, G., Lloyd-Hughes, B., Brayshaw, D. J., & Wade, A. J. (2013). Future changes in atmospheric rivers and their implications for winter flooding in Britain. *Environmental Research Letters*, *8*(3), 34010.

Lee, J., Choi, J., Lee, O., Yoon, J., & Kim, S. (2017). Estimation of Probable Maximum Precipitation in Korea using a Regional Climate Model. *Water*, *9*(4), 240.

Leung, L. R., & Qian, Y. (2009). Atmospheric rivers induced heavy precipitation and flooding in the western U.S. simulated by the WRF regional climate model. *Geophysical Research Letters*, *36*, L03820. https://doi.org/10.1029/2008GL036445

Li, X., Zhou, W., & Chen, Y. D. (2016). Detecting the origins of moisture over southeast China: Seasonal variation and heavy rainfall. *Advances in Atmospheric Sciences*, *33*(3), 319–329. https://doi.org/10.1007/s00376-015-4197-5

Liu, C., Ikeda, K., Rasmussen, R., Barlage, M., Newman, A. J., Prein, A. F., . . . Yates, D. (2017). Continental-scale convection-permitting modeling of the current and future climate of North America. *Climate Dynamics*, *49*(1), 71–95. https://doi.org/10.1007/s00382-016-3327-9

Lu, J., Ruby Leung, L., Yang, Q., Chen, G., Collins, W. D., Li, F., . . . Feng, X. (2014). The robust dynamical contribution to precipitation extremes in idealized warming simulations across model resolutions. *Geophysical Research Letters*, *41*, 2971–2978. https://doi.org/10.1002/2014GL059532

Micovic, Z., Schaefer, M. G., & Taylor, G. H. (2015). Uncertainty analysis for Probable Maximum Precipitation estimates. *Journal of Hydrology*, *521*, 360–373. https://doi.org/10.1016/j.jhydrol.2014.12.033

Mote, P., Brekke, L., Duffy, P. B., & Maurer, E. (2011). Guidelines for constructing climate scenarios. *Eos, Transactions American Geophysical Union*, *92*(31), 257–264. https://doi.org/10.1029/2011EO310001

Neiman, P. J., Schick, L. J., Ralph, F. M., Hughes, M., & Wick, G. A. (2011). Flooding in Western Washington: The connection to atmospheric rivers. *Journal of Hydrometeorology*, *12*(6), 1337–1358. https://doi.org/10.1175/2011JHM1358.1

Ngan, F., Stein, A., & Draxler, R. (2015). Inline coupling of WRF-HYSPLIT: Model development and evaluation using tracer experiments. *Journal of Applied Meteorology and Climatology*, *54*(6), 1162–1176. https://doi.org/10.1175/JAMC-D-14-0247.1

Numaguti, A. (1999). Origin and recycling processes of precipitating water over the Eurasian continent: Experiments using an atmospheric general circulation model. *Journal of Geophysical Research*, *104*(D2), 1957–1972. https://doi.org/10.1029/1998JD200026

Ohara, N., Kavvas, M., Kure, S., Chen, Z., & Jang, S. (2011). Physically based estimation of maximum precipitation over American River Watershed, California. *Journal of Hydrologic Engineering*, *16*(4), 351–361. https://doi.org/10.1061/(ASCE)HE.1943-5584.0000324

Pauluis, O. M. (2015). The global engine that could. *Science*, *347*(6221), 475–476. https://doi.org/10.1126/science.aaa3681

Peters, G. P., Andrew, R. M., Boden, T., Canadell, J. G., Ciais, P., Le Quéré, C., . . . Wilson, C. (2013). The challenge to keep global warming below 2°C. *Nature Climate Change*, *3*, 4–6. https://doi.org/10.1038/nclimate1766

Pfahl, S., O'Gorman, P. A., & Fischer, E. M. (2017). Understanding the regional pattern of projected future changes in extreme precipitation. *Nature Climate Change*, *7*, 423–427. https://doi.org/10.1038/nclimate3287

Pierce, D. W., Cayan, D. R., Maurer, E. P., Abatzoglou, J. T., & Hegewisch, K. C. (2015). Improved bias correction techniques for hydrological simulations of climate change. *Journal of Hydrometeorology*, *16*, 2421–2442. https://doi.org/10.1175/JHM-D-14-0236.1

Pierce, D. W., Cayan, D. R., & Thrasher, B. L. (2014). Statistical downscaling using Localized Constructed Analogs (LOCA). *Journal of Hydrometeorology*, *15*, 2558–2585. https://doi.org/10.1175/JHM-D-14-0082.1

Prein, A. F., Holland, G. J., Rasmussen, R. M., Done, J., Ikeda, K., Clark, M. P., & Liu, C. H. (2013). Importance of regional climate model grid spacing for the simulation of heavy precipitation in the Colorado Headwaters. *Journal of Climate*, *26*(13), 4848–4857. https://doi.org/10.1175/JCLI-D-12-00727.1

Rakhecha, P. R., & Kennedy, M. R. (1985). A generalised technique for the estimation of Probable Maximum Precipitation in India. *Journal of Hydrology*, *78*(3), 345–359. https://doi.org/10.1016/0022-1694(85)90112-X

Rakhecha, P. R., & Singh, V. P. (2009). *Applied hydrometeorology*. Berlin, Germany: Springer.

Ralph, F. M., Neiman, P. J., Kiladis, G. N., Weickmann, K., & Reynolds, D. W. (2011). A multiscale observational case study of a Pacific atmospheric river exhibiting tropical–extratropical connections and a mesoscale frontal wave. *Monthly Weather Review*, *139*(4), 1169–1189. https://doi.org/10.1175/2010MWR3596.1

Rastogi, D., Kao, S.-C., Ashfaq, M., Mei, R., Kabela, E. D., Gangrade, S., . . . Anantharaj, V. G. (2017). Effects of climate change on Probable Maximum Precipitation: A sensitivity study over the Alabama-Coosa-Tallapoosa River Basin. *Journal of Geophysical Research: Atmospheres*, *122*, 4808–4828. https://doi.org/10.1002/2016JD026001

Reynolds, R. W., Smith, T. M., Liu, C., Chelton, D. B., Casey, K. S., & Schlax, M. G. (2007). Daily high-resolution-blended analyses for sea surface temperature. *Journal of Climate*, *20*(22), 5473–5496. https://doi.org/10.1175/2007JCLI1824.1

Rouhani, H., & Leconte, R. (2016). A novel method to estimate the maximization ratio of the Probable Maximum Precipitation (PMP) using regional climate model output. *Water Resources Research*, *52*, 7347–7365. https://doi.org/10.1002/2016WR018603

Rousseau, A. N., Klein, I. M., Freudiger, D., Gagnon, P., Frigon, A., & Ratté-Fortin, C. (2014). Development of a methodology to evaluate Probable Maximum Precipitation (PMP) under changing climate conditions: Application to southern Quebec, Canada. *Journal of Hydrology*, *519*, 3094–3109. https://doi.org/10.1016/j.jhydrol.2014.10.053

Rupp, D. E., Abatzoglou, J. T., Hegewisch, K. C., & Mote, P. W. (2013). Evaluation of CMIP5 20th century climate simulations for the Pacific Northwest USA. *Journal of Geophysical Research: Atmospheres*, *118*, 10884–10906. https://doi.org/10.1002/jgrd.50843

Salas, J. D., Gavilán, G., Salas, F. R., Julien, P. Y., & Abdullah, J. (2014). Uncertainty of the PMP and PMF. In *Handbook of engineering hydrology: Modeling, climate change, and variability B. II* (pp. 575–603). Boca Raton, FL: CRC Press.

Schreiner, L. C., & Riedel, J. T. (1978). *Probable Maximum Precipitation estimates, United States east of the 105th meridian*. Silver Spring, MD: Department of Commerce, National Oceanic and Atmospheric Administration.

Seaber, P. R., Kapinos, F. P., & Knapp, G. L. (1987). Hydrologic unit maps. In *U.S. Geological Survey water supply paper* (63 pp.). Reston, VA: U.S. Geological Survey. Retrieved from http://pubs.usgs.gov/wsp/wsp2294/pdf/wsp_2294.pdf

Sheffield, J., Barrett, A. P., Colle, B., Fernando, D. N., Fu, R., Geil, K. L., . . . Yin, L. (2013). North American climate in CMIP5 experiments. Part I: Evaluation of historical simulations of continental and regional climatology. *Journal of Climate*, *26*(23), 9209–9245. https://doi.org/10.1175/JCLI-D-12-00592.1

Siler, N., & Roe, G. (2014). How will orographic precipitation respond to surface warming? An idealized thermodynamic perspective. *Geophysical Research Letters*, *41*, 2606–2613. https://doi.org/10.1002/2013GL059095

Stein, A. F., Draxler, R. R., Rolph, G. D., Stunder, B. J. B., Cohen, M. D., & Ngan, F. (2015). Noaa's hysplit atmospheric transport and dispersion modeling system. *Bulletin of the American Meteorological Society*, *96*(12), 2059–2077. https://doi.org/10.1175/BAMS-D-14-00110.1

AGU **Water Resources Research** 10.1002/2017WR021094

Stein, A. F., Isakov, V., Godowitch, J., & Draxler, R. R. (2007). A hybrid modeling approach to resolve pollutant concentrations in an urban area. *Atmospheric Environment*, *41*(40), 9410–9426. https://doi.org/10.1016/j.atmosenv.2007.09.004

Tan, E. (2010). *Development of a methodology for Probable Maximum Precipitation estimation over the American river watershed using the WRF model*. Davis: University of California, Davis.

Tarroja, B., AghaKouchak, A., & Samuelsen, S. (2016). Quantifying climate change impacts on hydropower generation and implications on electric grid greenhouse gas emissions and operation. *Energy*, *111*, 295–305. https://doi.org/10.1016/j.energy.2016.05.131

Trenberth, K. E., Dai, A., Rasmussen, R. M., & Parsons, D. B. (2003). The changing character of precipitation. *Bulletin of the American Meteorological Society*, *84*(9), 1205–1217. https://doi.org/10.1175/BAMS-84-9-1205

Vahedifard, F., AghaKouchak, A., Ragno, E., Shahrokhabadi, S., & Mallakpour, I. (2017). Lessons from the Oroville Dam. *Science*, *355*(6330), 1139–1140. https://doi.org/10.1126/science.aan0171

Warner, M. D., Mass, C. F., & Salathé, E. P., Jr. (2015). Changes in winter atmospheric rivers along the North American West Coast in CMIP5 climate models. *Journal of Hydrometeorology*, *16*(1), 118–128. https://doi.org/10.1175/JHM-D-14-0080.1

Wi, S., Valdés, J. B., Steinschneider, S., & Kim, T.-W. (2016). Non-stationary frequency analysis of extreme precipitation in South Korea using peaks-over-threshold and annual maxima. *Stochastic Environmental Research and Risk Assessment*, *30*(2), 583–606. https://doi.org/10.1007/s00477-015-1180-8

World Meteorological Organization (WMO). (1986). *Manual for estimation of Probable Maximum Precipitation* (Oper. Hydrol. Rep. 1, 2nd ed., Publ. 332). Geneva, Switzerland: Author.

Wu, H., Kimball, J. S., Li, H., Huang, M., Leung, L. R., & Adler, R. F. (2012). A new global river network database for macroscale hydrologic modeling. *Water Resources Research*, *48*, W09701. https://doi.org/10.1029/2012WR012313